

# Vibration Behavior of a Sandwich Porous Elliptical Micro-Shell with a Magneto-Rheological Core Based on the Modified Couple Stress Theory

A. Mohammadpour, S. Jafari Mehrabadi\*, P. Yousefi  
and H. Mohseni Monfared

*Department of Mechanical Engineering, Islamic Azad University, Arak Branch. Arak, Iran*

Received 1 July 2022; Accepted (in revised version) 7 December 2022

---

**Abstract.** Recently, the use of porous materials has grown widely in many structures, such as beams, plates, and shells. The characteristics of porous materials change in the thickness direction by different functions. This study has investigated the free vibration analysis of a sandwich porous elliptical micro-shell with a magneto-rheological fluid (MRF) core for the first time. Initially, we examined the displacement of the middle layer's macro- and micro-components, using Love's shell theory. Next, we used the modified couple stress theory (MCST) to obtain the strain and symmetrical curvature tensors for the three layers. The Hamilton's principle was implemented to derive the equations of motion. We also used the Galerkin's method to solve the equations of motion, resulting in a system of equations in the form of a linear eigenvalue problem. By solving the governing equations, we obtained the various natural frequencies and loss factors of the elliptical micro-shell, and compared them with the results in earlier studies. Lastly, we investigated the effects of thickness, porosity distribution pattern, aspect ratio, length scale parameter, and magnetic field intensity on the natural frequency and loss factor of the micro-shell. The data accuracy was validated by comparing them with those of reputable previous articles.

**AMS subject classifications:** 74-11

**Key words:** Elliptical micro shell, free vibration, magneto-rheological core, modified couple stress theory, sandwich porous material.

---

## 1 Introduction

Elliptical cylindrical shells are a particular type of structural element in engineering. The vibration of elliptical cylindrical shells is more critical than many other cylindrical structures. These structures are commonly used in acoustic transducers, submarine vehicles,

---

\*Corresponding author.

*Email:* sjmamir@gmail.com (S. Jafari Mehrabadi)

aircraft wings, fuselages, acoustic mufflers, and other similar structures. An extensive review, which has been published by Liessa [1], addresses the vibration of shells, including circular cylindrical shells. In recent years, Quato [2] published a review of more recent articles on similar shells. However, few studies have been conducted to date on the vibrational behavior of elliptical, cylindrical shells.

The vibration equations of elliptical, cylindrical shells are partial differential equations (PDEs) with variable coefficients of radius and circumferential curvature, making it more challenging to solve the analytical vibration problems of elliptical cylindrical shells than circular cylindrical shells. To overcome the difficulty of analysis, numerical methods have been applied to the analysis of the vibration behavior of elliptical, cylindrical shells. Shirakawa and Morita [3] considered the cross-section of the ellipse as two interconnected pieces of one circular arc. In their study, they employed the equations of circular, cylindrical shells to analyze vibration behavior of elliptical cylindrical shells. Further, the natural frequency of elliptical cylindrical shell are determined by assuming the continuous conditions of two pieces of the circular arcs. However, this method is very complicated due to the high-order partial derivatives. Hence the reason for undertaking the current study. After presenting the aim of the study, this article provides a careful review of the pertinent literature to familiarize the readers with the state-of-the-art studies on the subject.

## 1.1 Aim of the study

Considering the growing use of the functionally graded (FG) porous materials and their significant impact on controlling the free vibration behavior of FG porous elliptical microshells and the scarcity of research findings on this subject, we aimed to investigate a novel structural model as a porous elliptical micro-shell with a magneto-rheological core. The innovative objectives of this study were the impact of shell thickness, porosity distribution pattern, aspect ratios, length scale parameter, and magnetic field intensity on the natural frequencies and the loss factors, based on the modified couple stress theory (MCST), Hamilton's principle and Galerkin's method. Briefly, our promising results provide first-hand evidence that the material length scale and porosity parameters, geometry, wave number, cross-sectional, elliptical ratios, and magnetic field intensity all impact the structure's natural frequency and loss factor. These will be presented and discussed following a review of the literature.

## 1.2 Literature review

Klosner and Pohle [4,5] used a perturbation method to examine the vibration behavior of elliptical, cylindrical shells. However, this method can only be applicable for shells with a small elliptical parameter. Yamada, et al. [6] derived the equations for elliptical, cylindrical shells, using Sanders' shell theory and the principle of energy change, implementing the Ritz method to derive the natural frequency of their elliptical shell. Based

on the thick layer theory, Suzuki, et al. [7] investigated the effect of shear deformation and rotational inertia on the free vibration behavior of thick-walled elliptical, cylindrical shells. Further, Ganapathi, et al. [8] applied the finite element method (FEM) to the analysis of the flexural free vibration behavior of multilayer composite elliptical, cylindrical shells. In this context, Grigorenko, et al. [9] used the spline collision method to study the free vibration behavior of isotropic cylindrical shells with specific thicknesses. Also, Khalifa [10, 11] examined the vibration behavior of orthotropic and isotropic elliptical, cylindrical shells in two separate studies. The first one [10], focused on the effects of wave parameters on the vibration behavior, using transfer matrix and Romberg integration methods. The second study [11] utilized transfer matrix method to analyze the vibration behavior of elliptical, cylindrical shells, which were non-homogeneous orthotropic models with non-uniform Winkler's substrates. Tornabene, et al. [12, 13] employed a generalized differential quadrature method (GDQM) to study the free vibration characteristics of thick-walled elliptical, cylinders and thin-walled shells made of multi-layered composite materials.

### 1.2.1 Effect of functionally graded material

In previous studies, the vibration behavior of isotropic, orthotropic, and composite elliptical, cylindrical shells has been investigated [1–13]. In this context, FG materials are microscopically heterogeneous, and their mechanical characteristics vary from one layer to another. These novel materials are created by the functional distribution of internal pores to improve the structural efficiency. Some of the previous studies have analyzed the vibration behavior of FG cylindrical shells [14–17]. The earlier studies; however, did not examine the significance of porosity and its distribution in FG materials. When porosity occurs within the material in the process of fabricating FG materials, it is crucial to consider its effects on the shells' vibration behavior.

Among others, previous have examined the vibration behavior of FG material beams made of porous materials [18, 19]. Functionally graded materials in micro- or nanostructures, such as atomic force microscopes and similar devices have had significant impact on mechanical engineering research in recent years. Studies have demonstrated that the stiffness and strength of micro- or nano-structures are greater than those of the macro models [18–20]. The classical theory of continuous systems cannot provide the size effects. For this reason, specific shear deformation theories, i.e., micropolar [20], displacement, plane elasticity [21, 22], gradient and modified couple stress theories (MCST) [23, 24] have been used to examine the size effects.

### 1.2.2 Buckling and bending versus vibration

Coskun, et al. [25] analyzed the buckling, bending, and vibration of FG porous microshells, using the third-order shear deformation theory. The equations of motion of an FG microshell were achieved via MCST and Hamilton's principle. These authors considered three different distribution patterns to demonstrate the porosity types. Further,

the effect of porosity features and the material length scale versus the mechanical behavior of microshells was studied, using the Navier's solution. Kim, et al. [26] analyzed the buckling, bending, and vibration of FG porous microshells, utilizing the first-order shear deformation theory. Also, MCST was employed to respect the effects of size on the micro-scale. Ghadiri and Safarpour [27] studied the size effects versus the free vibration behavior of an FG porous cylindrical, microshell in a thermal environment based on the first order shear deformation theory (FSDT) and MCST. They employed the minimum potential energy principle to derive the equations of motion. These authors investigated the effects of length scale, porosity volume fraction, and the longitudinal and circumferential wave number on the free vibration behavior of microshells.

Afshari and Adab [28] used the quasi-3D sinusoidal shear deformation theory (SSDT) along with MCST to study the size-dependent mechanical buckling and free vibration of microplates reinforced with graphene nanoplatelets (GNPs). Adab, et al. [29] utilized FSDT and MCST to analyze the free vibration of a rotating truncated sandwich conical microshell with an FGP core and GNP-reinforced face sheets. These authors demonstrated that the highest natural frequencies can be achieved when the large pores are located near the middle surface of the microshell.

### 1.2.3 Geometry versus piezoelectric and piezomagnetic effects

Gholami and Ansari [43] investigated the geometrical, nonlinear free vibration behavior of piezoelectric and piezomagnetic nanobeams subjected to magneto-electro-thermal loading, versus the effect, based on the nonlocal elasticity theory. The size-dependent nonlinear governing equations of motion and the corresponding boundary conditions were derived based on the nonlocal elasticity and first-order shear deformation theories with von Karman-type of kinematic nonlinearity. In this study, the effects of size-dependence, shear deformations, rotary inertia, piezoelectric or piezomagnetic coupling, thermal environment, and geometrical nonlinearity were also examined. They also used the generalized differential quadrature (GDQ) method in conjunction with the numerical Galerkin method, periodic time differential operators and pseudo arc length continuation method to compute the nonlinear frequency response for piezoelectric or piezomagnetic nanobeams.

### 1.2.4 Porosity versus viscoelastic materials

Jalaei and Civalek [44] studied the transient response of porosity-dependent viscoelastic FG nanobeams, subjected to dynamic loads and magnetic field. The material properties of the beams with gradual variations along the thickness direction were analyzed based on modified power-law function. This study used nonlocal strain gradient theory (NSGT) based on a quasi-3D beam theory and the thickness stretching effect. The authors applied the Kelvin-Voigt visco-constitutive model to examine the internal damping effect. Also, they derived the governing equations based on the Hamilton's, Navier's and inverse Laplace transform methods. In addition, these authors performed parametric analyses to determine the sensitivity of the transient response to porosity coefficient,

internal damping, volume fraction, length to thickness ratio, point load, magnetic field, and small size variables.

### 1.2.5 Forced vibration carbon nanotubes versus harmonic point load

Civalek and Akbas [45] studied the forced vibration analysis of simply supported beam made of carbon nanotube and reinforced composite material subjected to a harmonic point load. This study applied the FSDT and Lagrange procedure to derive the governing equations. Also, the problem was solved, using the Ritz method with the variables being the effect of carbon nanotube volume fraction, aspect ratio and dynamic parameters related to the forced vibration response. Liew and Lim [46] investigated the modeling of vibratory response of varying thicknesses versus cantilevered shallow cylindrical shells. The equations of motion were derived based on the principle of minimum total energy. In this study, a basic approximation method was introduced to satisfy the kinetic boundary conditions. Soleimani, et al. [47] studied a new cylindrical shell element, based on modified couple stress theory instead of classical continuum theory. They examined the vibration and buckling behaviors of nanotubes via the finite element method. In addition, they investigated such variables, as cylindrical shell elements, mass-stiffness matrix, super, and size-dependent finite elements. Also, the shell elements were extended to accurately account for nano-tube vibration and buckling features. The new cylindrical shell elements had been developed based on the function of super element's shape. In order to test the application of the equations, they focused on the cylindrical nano-shell bending displacement, based on the modified couple stress cylindrical shell element, and the results validated based on analytical method. In addition, the effects of such variables, as length scale parameter, length, and thickness on cylindrical shell displacement were investigated. The results indicated that the super element considerably reduced the computation processes and time compared to using molecular dynamic simulation.

## 2 Materials and methods

### 2.1 Porous material characteristics

Fig. 1 illustrates a schematic elliptical cylindrical microshell. The radius, thickness and length of the microshell are  $R$ ,  $h$ ,  $L$ , respectively. The used coordinate system is represented for elliptical cylindrical microshell as  $(x, \theta, z)$ . Sequentially, displacements in  $x$ ,  $\theta$ , and  $z$  directions are shown by  $u$ ,  $v$ , and  $w$ .

As shown in Fig. 2 below, two different distribution patterns of the porous material were considered, exhibited by the distribution pattern. The symmetrical distribution is represented in panel A while the non-symmetrical distribution is designated in panel B.

The following equations express variations in the elastic modulus ( $E$ ), shear modulus

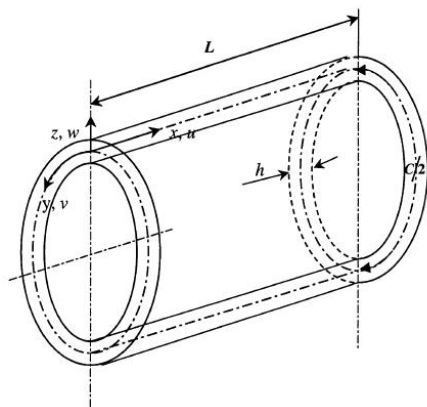


Figure 1: Geometry of the elliptical cylindrical microshell.

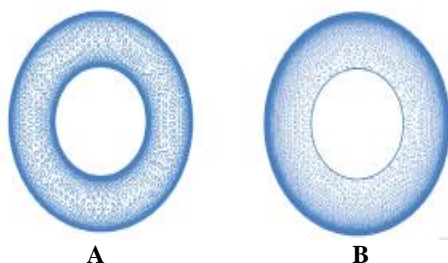


Figure 2: The distribution patterns of the porous material. A: Symmetrical distribution, B: Asymmetrical distribution.

(G) and material density ( $\rho$ ):

$$\left\{ \begin{array}{l} \text{Type1:(symmetricdistribution),} \\ E(z) = E_0 \left[ 1 - e_0 \cos\left(\frac{\pi z}{h}\right) \right], \\ G(z) = G_0 \left[ 1 - e_0 \cos\left(\frac{\pi z}{h}\right) \right], \\ \rho(z) = \rho_0 \left[ 1 - e_m \cos\left(\frac{\pi z}{h}\right) \right], \end{array} \right. \quad \left\{ \begin{array}{l} \text{Type2:(Asymmetricdistribution),} \\ E(z) = E_0 \left[ 1 - e_0 \cos\left(\frac{\pi z}{2h} + \frac{\pi}{4}\right) \right], \\ G(z) = G_0 \left[ 1 - e_0 \cos\left(\frac{\pi z}{2h} + \frac{\pi}{4}\right) \right], \\ \rho(z) = \rho_0 \left[ 1 - e_m \cos\left(\frac{\pi z}{2h} + \frac{\pi}{4}\right) \right], \end{array} \right. \quad (2.1)$$

in which the porosity parameter is stated as  $0 \leq e_0 = 1 - \frac{E_0}{E_1} = 1 - \frac{G_0}{G_1} < 1$ , in which  $E_0$  and  $E_1$  are the lowest and the highest values of elastic modulus in the thickness direction, respectively. The porosity parameter in terms of mass density is defined as  $0 \leq e_m = 1 - \frac{\rho_0}{\rho_1} < 1$ , where  $\rho_0$  and  $\rho_1$  are the lowest and highest amount of mass density in the thickness direction, sequentially  $e_0$  and  $e_m$  are related as follow:

$$e_m = 1 - \sqrt{1 - e_0}. \quad (2.2)$$

## 2.2 Modified couple stress theory

This theory is one of the higher order models [36–39] where the strain energy is dependent on the strain and its variations. In these theories, the higher order rotation gradient is considered in deformation equations. Mindlin rewrote this theory to encompass the higher order strain gradient [40]. Fleck and Hutchinson simplified the theory developed by Mindlin and termed it "strain gradient theory" [41]. However, Lam, et al. revised the theory, and eliminated the asymmetric section of the strain gradient tensor. The modified theory has only three constants for the effect of MLS parameter to replace the old five constants considered by Mindlin. By setting two out of the three MLS parameters to zero, the couple stress theory takes the following form [10, 42]

$$U = \frac{1}{2} \int_V (\sigma_{ij} \varepsilon_{ij} + m_{ij} \chi_{ij}). \quad (2.3)$$

Where  $\varepsilon_{ij}$ ,  $\sigma_{ij}$ ,  $\chi_{ij}$  and  $m_{ij}$  are the components of strain and Cauchy stress tensors, and the symmetrical rotation gradient tensor at higher order stress, respectively, which are defined as follows:

$$\varepsilon_{ij} = \frac{1}{2} (u_{i,j} + u_{j,i}), \quad \sigma_{ij} = C_{ijkl} \varepsilon_{kl}, \quad (2.4a)$$

$$\chi_{ij} = \frac{1}{4} (e_{ipq} \eta_{j pq} + e_{j pq} \eta_{i pq}), \quad \eta_{ijk} = u_{k,ij}, \quad m_{ij} = 2\mu l \chi_{ij}, \quad (2.4b)$$

where  $u$  and  $\eta$  are the displacement vector and second-order displacement gradient tensor, respectively. In Eq. (2.4),  $l$  is the length scale parameter. Also,  $\mu$  represents the shear modulus and is defined as follows:

$$\mu = \frac{E}{2(1+\nu)}. \quad (2.5)$$

## 2.3 Magnetorhological material characteristics

In several earlier studies, the MRF shear modulus has been described based on the shear stress-strain properties, characterized by two distinct zones, termed as the pre-yield and post-yield. Although the utilized magnetic field has a significant impact on the shear stress-strain characteristics of the MRF material, the determined characteristics generally exhibit comparable patterns. The viscoelastic behavior of the MRF materials, described in terms of complex modulus  $G^*$ , is defined as follows in the pre-yield zone

$$G^* = G' + iG''. \quad (2.6)$$

Where,  $G'$  and  $G''$  are the storage and loss factor moduli of the MRF, respectively. Of note, the  $G'$  and  $G''$  are related to the average energy stored and a measure of the energy

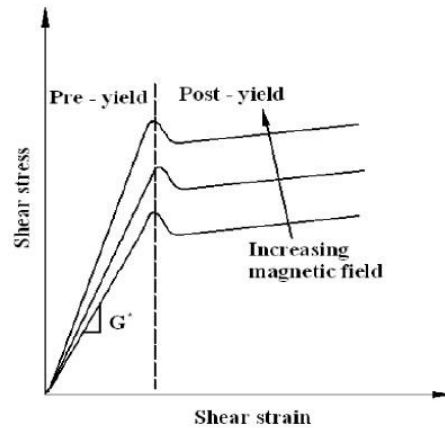


Figure 3: The shear stress-strain relationship of MRF materials under varying intensities of magnetic field.

dissipated per unit volume of the material over a deformation cycle, respectively. The functions of  $G'$  and  $G''$  in the MRF are assumed as follows:

$$G'(B) = -3.3691B^2 + 4.9975 \times 10^3 B + 0.893 \times 10^6, \quad (2.7a)$$

$$G''(B) = -0.9B^2 + 0.8124 \times 10^3 B + 0.1855 \times 10^6. \quad (2.7b)$$

Where  $B$  is the magnetic field intensity in gauss ( $G$ ):

## 2.4 Theoretical formulation

The following assumptions are made to derive the equations of motion:

- The only layer which is subjected to the shear deformation is the middle MRF layer.
- The only thing which affects the material characteristics of the middle MRF layer is the magnetic field.
- A specific mix modulus is used to define the material behavior in the middle MRF layer.
- Variations in the transverse displacement in the thickness direction are negligible.
- A no-slip condition is assumed among the three layers.
- There is no normal stress in the middle layer, thus, only the effect of shear stress is considered.

Sequentially, the geometry and deformation distribution of the microshell are displayed in Fig. 4. The  $z$  coordinate is perpendicular to the plane of the microshell.

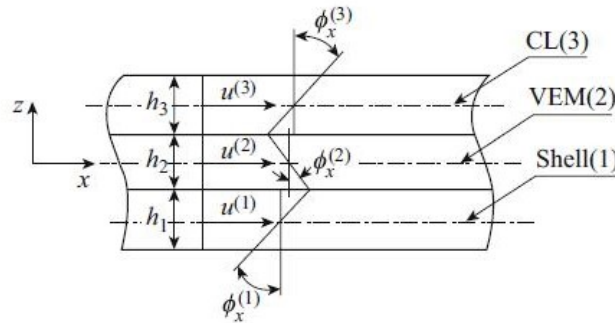


Figure 4: Deformation distribution and continuity of the sandwich microshell.

According to Donnell assumptions for upper and lower layers of the plate, the displacement field is considered as follows ( $i = 1,3$ ):

$$U_i(x, \theta, z, t) = u_i(x, \theta, t) - z_i \frac{\partial w_i(x, \theta, t)}{\partial x}, \tag{2.8a}$$

$$V_i(x, \theta, z, t) = v_i(x, \theta, t) - \frac{z_i}{R(\theta)} \left( \frac{\partial w_i(x, \theta, t)}{\partial \theta} - v_i(x, \theta, t) \right), \tag{2.8b}$$

$$W_i(x, \theta, z, t) = w(x, \theta, t), \tag{2.8c}$$

the displacement field of the middle core of MRF is assumed based on the FSDT as:

$$U_2(x, \theta, z, t) = u_2(x, \theta, t) + z_2 \varphi_2(x, \theta, t), \tag{2.9a}$$

$$V_2(x, \theta, z, t) = v_2(x, \theta, t) + z_2 \psi_2(x, \theta, t), \tag{2.9b}$$

$$W_2(x, \theta, z, t) = w(x, \theta, t). \tag{2.9c}$$

Where,  $-\frac{h_i}{2} \leq z_i \leq \frac{h_i}{2}$  and  $h_i$  is the thickness of  $i$ th layer. The following equations are stated based on the continuity conditions:

$$U_1|_{z_1=\frac{h_1}{2}} = U_2|_{z_2=-\frac{h_2}{2}}, \quad U_3|_{z_3=-\frac{h_3}{2}} = U_2|_{z_2=\frac{h_2}{2}}, \tag{2.10a}$$

$$V_1|_{z_1=\frac{h_1}{2}} = V_2|_{z_2=-\frac{h_2}{2}}, \quad V_3|_{z_3=-\frac{h_3}{2}} = V_2|_{z_2=\frac{h_2}{2}}, \tag{2.10b}$$

using Eqs. (2.8)-(2.10), displacement components of the middle MRF layer are stated as:

$$u_2(x, \theta, t) = \left( \frac{u_1 + u_3}{2} \right) + \left( \frac{h_3 - h_1}{4} \right) \frac{\partial w}{\partial x}, \quad \varphi_2(x, \theta, t) = \left( \frac{u_3 - u_1}{h_2} \right) + \left( \frac{h_1 + h_3}{2h_2} \right) \frac{\partial w}{\partial x}, \tag{2.11a}$$

$$v_2(x, \theta, t) = \left( \frac{v_1 + v_3}{2} \right) + \left( \frac{h_3 - h_1}{4R(\theta)} \right) \frac{\partial w}{\partial \theta}, \quad \psi_2(x, \theta, t) = \left( \frac{v_3 - v_1}{h_2} \right) + \left( \frac{h_1 + h_3}{2h_2R(\theta)} \right) \frac{\partial w}{\partial \theta}. \tag{2.11b}$$

The linear components of shear and normal strain in double-curved coordinate are defined as follows:

$$\varepsilon_i = \frac{\partial}{\partial \xi_i} \left( \frac{U_i}{A_i} \right) + \frac{1}{A_i} \sum_{k=1}^3 \frac{U_k}{A_k} \frac{\partial A_i}{\partial \xi_k}, \tag{2.12a}$$

$$\gamma_{ij} = \frac{1}{A_i A_j} \left[ A_i^2 \frac{\partial}{\partial \xi_j} \left( \frac{U_i}{A_i} \right) + A_j^2 \frac{\partial}{\partial \xi_i} \left( \frac{U_j}{A_j} \right) \right], \quad i, j = 1, 2, 3, \quad i \neq j. \tag{2.12b}$$

By simplifying the relations in Eq. (2.12), the linear components of normal strain in double-curved coordinates are stated as:

$$\varepsilon_1 = \frac{1}{A_1} \left[ \frac{\partial U_1}{\partial x_1} + \frac{1}{A_2} \frac{\partial A_1}{\partial x_2} U_2 + \frac{A_1}{R_1} U_3 \right], \tag{2.13a}$$

$$\varepsilon_2 = \frac{1}{A_2} \left[ \frac{\partial U_2}{\partial x_2} + \frac{1}{A_1} \frac{\partial A_2}{\partial x_1} U_1 + \frac{A_2}{R_2} U_3 \right], \quad \varepsilon_3 = \frac{\partial U_3}{\partial x_3}, \tag{2.13b}$$

$$\gamma_{23} = \frac{1}{A_2} \frac{\partial U_3}{\partial x_2} + A_2 \frac{\partial}{\partial x_3} \left( \frac{U_2}{A_2} \right), \tag{2.13c}$$

$$\gamma_{13} = \frac{1}{A_1} \frac{\partial U_3}{\partial x_1} + A_1 \frac{\partial}{\partial x_3} \left( \frac{U_1}{A_1} \right), \tag{2.13d}$$

$$\gamma_{12} = \frac{A_2}{A_1} \frac{\partial}{\partial x_1} \left( \frac{U_2}{A_2} \right) + \frac{A_1}{A_2} \frac{\partial}{\partial x_2} \left( \frac{U_1}{A_1} \right). \tag{2.13e}$$

The Lamé’s constants and the curvature radius of the elliptical shell are expressed as follows:

$$A_1 = 1, \quad A_2 = R(\theta), \tag{2.14a}$$

$$R_1 = \infty, \quad R_2 = R(\theta). \tag{2.14b}$$

The mechanical strain components are achieved by substituting the Lamé’s constant and the curvature radius of the elliptical shell of Eq. (2.14) within the displacement strain relations of Eq. (2.10):

$$\varepsilon_x = \frac{\partial U}{\partial x}, \quad \varepsilon_\theta = \frac{1}{R(\theta)} \left[ \frac{\partial V}{\partial \theta} + W \right], \quad \varepsilon_z = \frac{\partial W}{\partial z}, \tag{2.15a}$$

$$\gamma_{\theta z} = \frac{1}{R(\theta)} \frac{\partial W}{\partial \theta} - \frac{V}{R(\theta)} + \frac{\partial V}{\partial z} = 2\varepsilon_4, \tag{2.15b}$$

$$\gamma_{xz} = \frac{\partial W}{\partial x} + \frac{\partial U}{\partial z} = 2\varepsilon_5, \tag{2.15c}$$

$$\gamma_{x\theta} = \frac{\partial V}{\partial x} + \frac{1}{R(\theta)} \frac{\partial U}{\partial \theta} = 2\varepsilon_6. \tag{2.15d}$$

By substituting the displacement field of Eq. (2.8) into the displacement strain relations of Eq. (2.15), the Green Lagrange strain tensor components for the upper and lower layers

are obtained as follows ( $i = 1, 3$ ):

$$\varepsilon_{xx}^{(i)} = \frac{\partial u_i}{\partial x} - z_i \frac{\partial^2 w}{\partial x^2}, \tag{2.16a}$$

$$\begin{aligned} \varepsilon_{\theta\theta}^{(i)} = & \frac{1}{R(\theta)} \frac{\partial v_i}{\partial \theta} + \frac{z_i}{R(\theta)^2} \frac{\partial v_i}{\partial \theta} + \frac{w}{R(\theta)} - \frac{z_i}{R(\theta)^2} \frac{\partial^2 w}{\partial \theta^2} \\ & + \frac{z_i}{R(\theta)^3} \left( \frac{dR(\theta)}{d\theta} \right) \frac{\partial w}{\partial \theta} - \frac{z_i}{R(\theta)^3} \left( \frac{dR(\theta)}{d\theta} \right) v_i, \end{aligned} \tag{2.16b}$$

$$\varepsilon_{zz}^{(i)} = 0, \quad \gamma_{\theta z}^{(i)} = 0, \quad \gamma_{xz}^{(i)} = 0, \tag{2.16c}$$

$$\gamma_{x\theta}^{(i)} = \frac{\partial v_i}{\partial x} + \frac{z_i}{R(\theta)} \frac{\partial v_i}{\partial x} + \frac{1}{R(\theta)} \frac{\partial u_i}{\partial \theta} - \frac{2z_i}{R(\theta)} \frac{\partial^2 w}{\partial x \partial \theta}. \tag{2.16d}$$

Also, by substituting the displacement field of Eq. (2.9) into the displacement strain relations of Eq. (2.17), the shear components of the Green Lagrange strain tensor for the second layer are achieved as follows:

$$\begin{aligned} \gamma_{\theta z}^{(2)} = & \frac{1}{R(\theta)} \frac{\partial w}{\partial \theta} + \psi_2 - \frac{v_2}{R(\theta)} \\ = & \frac{v_3 - v_1}{h_2} - \frac{v_1 + v_3}{2R(\theta)} + \frac{1}{R(\theta)} \frac{\partial w}{\partial \theta} + \left( \frac{h_1 + h_3}{2h_2 R(\theta)} \right) \frac{\partial w}{\partial \theta} + \left( \frac{h_1 - h_3}{4R(\theta)^2} \right) \frac{\partial w}{\partial \theta}, \end{aligned} \tag{2.17a}$$

$$\gamma_{xz}^{(2)} = \frac{\partial w}{\partial x} + \varphi_2 = \frac{u_3 - u_1}{h_2} + \left( \frac{h_1 + h_3}{2h_2} \right) \frac{\partial w}{\partial x} + \frac{\partial w}{\partial x}. \tag{2.17b}$$

The non-zero components of mechanical strains of all three layers can be arranged as follows ( $i = 1, 3$ ):

$$\varepsilon_{xx_0}^{(i)} = \frac{\partial u_i}{\partial x}, \quad \varepsilon_{\theta\theta_0}^{(i)} = \frac{1}{R(\theta)} \frac{\partial v_i}{\partial \theta} + \frac{w}{R(\theta)}, \tag{2.18a}$$

$$\gamma_{x\theta_0}^{(i)} = \frac{\partial v_i}{\partial x} + \frac{1}{R(\theta)} \frac{\partial u_i}{\partial \theta}, \quad \varepsilon_{xx_1}^{(i)} = -\frac{\partial^2 w}{\partial x^2}, \tag{2.18b}$$

$$\varepsilon_{\theta\theta_1}^{(i)} = \frac{1}{R(\theta)^2} \frac{\partial v_i}{\partial \theta} - \frac{1}{R(\theta)^2} \frac{\partial^2 w}{\partial \theta^2} + \frac{1}{R(\theta)^3} \left( \frac{dR(\theta)}{d\theta} \right) \frac{\partial w}{\partial \theta} - \frac{1}{R(\theta)^3} \left( \frac{dR(\theta)}{d\theta} \right) v_i, \tag{2.18c}$$

$$\gamma_{x\theta_1}^{(i)} = \frac{1}{R(\theta)} \frac{\partial v_i}{\partial x} - \frac{2}{R(\theta)} \frac{\partial^2 w}{\partial x \partial \theta}, \tag{2.18d}$$

$$\gamma_{\theta z_0}^{(2)} = \frac{v_3 - v_1}{h_2} - \frac{v_1 + v_3}{2R(\theta)} + \frac{1}{R(\theta)} \frac{\partial w}{\partial \theta} + \left( \frac{h_1 + h_3}{2h_2 R(\theta)} \right) \frac{\partial w}{\partial \theta} + \left( \frac{h_1 - h_3}{4R(\theta)^2} \right) \frac{\partial w}{\partial \theta}, \tag{2.18e}$$

$$\gamma_{xz_0}^{(2)} = \frac{u_3 - u_1}{h_2} + \left( \frac{h_1 + h_3}{2h_2} \right) \frac{\partial w}{\partial x} + \frac{\partial w}{\partial x}. \tag{2.18f}$$

To compute the mechanical strain in micro scale, curvature tensor in MCST is used as [30]

$$\chi_{ij}^s = \frac{1}{4} (e_{ipq} \eta_{jpr} + e_{jpr} \eta_{ipq}). \tag{2.19}$$

Where  $e$  is the permutation symbol, and  $\eta$  represents the second-order deformation gradient tensor. The classical and non-classical strain relations are defined in the curvature coordinate system as [30]:

$$\begin{aligned} \varepsilon_{(j)}^{(i)} = \varepsilon_j^i \sqrt{\frac{g_{ii}}{g_{jj}}} = \frac{1}{2} \sqrt{\frac{g_{ii}}{g_{jj}}} \left\{ \left[ \left( \frac{u^{(i)}}{\sqrt{g_{ii}}} \right) + \Gamma_{nj}^i \frac{II^{(m)}}{\sqrt{g_{mm}}} \right] \right. \\ \left. + g_{nj} g^{im} \left[ \left( \frac{u^{(n)}}{\sqrt{g_{mm}}} \right) + \Gamma_{qm}^n \frac{u^{(q)}}{\sqrt{g_{qq}}} \right] \right\}, \end{aligned} \tag{2.20a}$$

$$\eta_{(i)(j)}^k = \eta_{ij}^k \sqrt{\frac{g_{kk}}{g_{ii}g_{jj}}} = \frac{1}{2} \sqrt{\frac{g_{kk}}{g_{ii}g_{jj}}} (u_{,ij}^k + u_{,ji}^k), \tag{2.20b}$$

$$\begin{aligned} u_{,lm}^k = \left( \frac{u^{(k)}}{\sqrt{g_{kk}}} \right)_{,lm} + \Gamma_{ql}^k \left( \frac{u^{(q)}}{\sqrt{g_{qq}}} \right)_{,m} + \Gamma_{qm}^k \left( \frac{u^{(q)}}{\sqrt{g_{qq}}} \right)_{,l} - \Gamma_{ml}^q \left( \frac{u^{(k)}}{\sqrt{g_{kk}}} \right)_{,q} \\ + \left[ (\Gamma_{lp}^k)_{,m} + \Gamma_{qm}^k \Gamma_{pl}^q - \Gamma_{pq}^k \Gamma_{ml}^q \right] \times \frac{u^p}{\sqrt{g_{pp}}}. \end{aligned} \tag{2.20c}$$

Where  $u$ ,  $\varepsilon$ , and  $\eta$  are the displacement vector, displacement gradient tensor, and second-order displacement gradient tensor. Also, in the above relation, the values of  $g$  and  $\Gamma$  are the covariance component of the Euclidean metric tensor and the second-order Christopher index, respectively.

In the cylindrical coordinate system, the Euclidean metric tensor and the second-order Christopher index components are as follows:

$$g_{xx} = 1, \quad g_{\theta\theta} = \left[ R \left( 1 + \frac{z}{R} \right) \right]^2, \quad g_{zz} = 1, \quad g_{kl} = 0, \quad (k \neq l), \tag{2.21a}$$

$$\Gamma_{z\theta}^\theta = \Gamma_{\theta z}^\theta = \left[ R \left( 1 + \frac{z}{R} \right) \right]^{-1}, \quad \Gamma_{\theta\theta}^z = -R \left( 1 + \frac{z}{R} \right), \tag{2.21b}$$

employing Eqs. (2.19)-(2.21) and Eq. (2.16), the symmetric curvature tensor components of the first and third layers are accomplished as follows ( $i=1,3$ ):

$$\chi_{xx}^{(i)} = \frac{1}{R(\theta)} \frac{\partial^2 w}{\partial x \partial \theta} - \frac{1}{R(\theta)} \frac{\partial v_i}{\partial x} + \frac{z_i}{2R(\theta)^2} \frac{\partial^2 w}{\partial x \partial \theta} - \frac{z_i}{2R(\theta)^2} \frac{\partial v_i}{\partial x}, \tag{2.22a}$$

$$\chi_{\theta\theta}^{(i)} = -\frac{1}{R(\theta)} \frac{\partial^2 w}{\partial x \partial \theta} - \frac{1}{2R(\theta)^2} \frac{\partial u_i}{\partial \theta} + \frac{1}{2R(\theta)} \frac{\partial v_i}{\partial x} + \frac{z_i}{2R(\theta)^2} \frac{\partial v_i}{\partial x}, \tag{2.22b}$$

$$\chi_{zz}^{(i)} = \frac{1}{2R(\theta)^2} \frac{\partial u_i}{\partial \theta} - \frac{z_i}{2R(\theta)^2} \frac{\partial^2 w}{\partial x \partial \theta} + \frac{1}{2R(\theta)} \frac{\partial v_i}{\partial x}, \tag{2.22c}$$

$$\chi_{xz}^{(i)} = -\frac{z_i}{4R(\theta)^3} \frac{\partial w}{\partial \theta} + \frac{z_i}{4R(\theta)^3} v_i - \frac{1}{4R(\theta)} \frac{\partial^2 u_i}{\partial x \partial \theta} + \frac{1}{4} \frac{\partial^2 v_i}{\partial x^2} + \frac{z_i}{4R(\theta)} \frac{\partial^2 v_i}{\partial x^2}, \tag{2.22d}$$

$$\begin{aligned} \chi_{\theta z}^{(i)} = & -\frac{1}{4R(\theta)^2} \frac{\partial^2 u_i}{\partial \theta^2} + \frac{1}{2R(\theta)} \frac{\partial w}{\partial x} + \frac{1}{4R(\theta)} \frac{\partial^2 v_i}{\partial x \partial \theta} + \frac{z_i}{4R(\theta)^3} \left( \frac{dR(\theta)}{d\theta} \right) \frac{\partial^2 w}{\partial x \partial \theta} \\ & - \frac{z_i}{4R(\theta)^3} \left( \frac{dR(\theta)}{d\theta} \right) \frac{\partial v_i}{\partial x} + \frac{z_i}{4R(\theta)^2} \frac{\partial^2 v_i}{\partial x \partial \theta}, \end{aligned} \quad (2.22e)$$

$$\begin{aligned} \chi_{x\theta}^{(i)} = & -\frac{1}{4R(\theta)^3} \left( \frac{dR(\theta)}{d\theta} \right) \frac{\partial w}{\partial \theta} + \frac{1}{4R(\theta)^3} \left( \frac{dR(\theta)}{d\theta} \right) v_i + \frac{1}{2R(\theta)^2} \frac{\partial^2 w}{\partial \theta^2} - \frac{z_i}{4R(\theta)^4} \left( \frac{dR(\theta)}{d\theta} \right) \frac{\partial w}{\partial \theta} \\ & + \frac{z_i}{4R(\theta)^4} \left( \frac{dR(\theta)}{d\theta} \right) v_i + \frac{z_i}{4R(\theta)^3} \frac{\partial^2 w}{\partial \theta^2} - \frac{z_i}{4R(\theta)^3} \frac{\partial v_i}{\partial \theta} - \frac{1}{2R(\theta)^2} \frac{\partial v_i}{\partial \theta} - \frac{1}{2} \frac{\partial^2 w}{\partial x^2}. \end{aligned} \quad (2.22f)$$

Also, using Eqs. (2.17), (2.19)-(2.21), the symmetric curvature tensor components of the second layer are stated as:

$$\chi_{xx}^{(2)} = -\frac{1}{2} \frac{\partial \psi_2}{\partial x} + \frac{1}{2R(\theta)} \frac{\partial^2 w}{\partial x \partial \theta} - \frac{1}{2R(\theta)} \frac{\partial v_2}{\partial x} - \frac{z_2}{2R(\theta)} \frac{\partial \psi_2}{\partial x}, \quad (2.23a)$$

$$\begin{aligned} \chi_{\theta\theta}^{(2)} = & \frac{1}{2R(\theta)} \frac{\partial \varphi_2}{\partial \theta} - \frac{1}{2R(\theta)^2} \frac{\partial u_2}{\partial \theta} - \frac{z_2}{2R(\theta)^2} \frac{\partial \varphi_2}{\partial \theta} - \frac{1}{2R(\theta)} \frac{\partial^2 w}{\partial x \partial \theta} \\ & + \frac{1}{2R(\theta)} \frac{\partial v_2}{\partial x} + \frac{z_2}{2R(\theta)} \frac{\partial \psi_2}{\partial x}, \end{aligned} \quad (2.23b)$$

$$\chi_{zz}^{(2)} = -\frac{1}{2R(\theta)} \frac{\partial \varphi_2}{\partial \theta} + \frac{1}{2R(\theta)^2} \frac{\partial u_2}{\partial \theta} + \frac{z_2}{2R(\theta)^2} \frac{\partial \varphi_2}{\partial \theta} + \frac{1}{2} \frac{\partial \psi_2}{\partial x}, \quad (2.23c)$$

$$\begin{aligned} \chi_{\theta z}^{(2)} = & -\frac{1}{4R(\theta)^2} \frac{\partial^2 u_2}{\partial \theta^2} - \frac{z_2}{4R(\theta)^2} \frac{\partial^2 \varphi_2}{\partial \theta^2} - \frac{\varphi_2}{4R(\theta)} + \frac{1}{4R(\theta)} \frac{\partial^2 v_2}{\partial x \partial \theta} \\ & + \frac{z_2}{4R(\theta)} \frac{\partial^2 \psi_2}{\partial x \partial \theta} + \frac{1}{4R(\theta)} \frac{\partial w}{\partial x}, \end{aligned} \quad (2.23d)$$

$$\begin{aligned} \chi_{xz}^{(2)} = & -\frac{1}{4R(\theta)^2} \frac{\partial w}{\partial \theta} - \frac{\psi_2}{4R(\theta)} + \frac{v_2}{4R(\theta)^2} + \frac{z_2}{4R(\theta)^2} \psi_2 - \frac{1}{4R(\theta)} \frac{\partial^2 u_2}{\partial x \partial \theta} \\ & - \frac{z_2}{4R(\theta)} \frac{\partial^2 \varphi_2}{\partial x \partial \theta} + \frac{1}{4} \frac{\partial^2 v_2}{\partial x^2} + \frac{z_2}{4} \frac{\partial^2 \psi_2}{\partial x^2}, \end{aligned} \quad (2.23e)$$

$$\chi_{x\theta}^{(2)} = -\frac{1}{4R(\theta)} \frac{\partial \psi_2}{\partial \theta} - \frac{1}{4R(\theta)^2} \frac{\partial v_2}{\partial \theta} - \frac{z_2}{4R(\theta)^2} \frac{\partial \psi_2}{\partial \theta} + \frac{1}{4R(\theta)^2} \frac{\partial^2 w}{\partial \theta^2} + \frac{1}{4} \frac{\partial \varphi_2}{\partial x} - \frac{1}{4} \frac{\partial^2 w}{\partial x^2}. \quad (2.23f)$$

The non-zero components of the symmetric curvature tensor of the three layers may be classified as follows ( $i=1,3$ ):

$$\chi_{xx_0}^{(i)} = \frac{1}{R(\theta)} \frac{\partial^2 w}{\partial x \partial \theta} - \frac{1}{R(\theta)} \frac{\partial v_i}{\partial x}, \quad \chi_{\theta\theta_0}^{(i)} = -\frac{1}{R(\theta)} \frac{\partial^2 w}{\partial x \partial \theta} - \frac{1}{2R(\theta)^2} \frac{\partial u_i}{\partial \theta} + \frac{1}{2R(\theta)} \frac{\partial v_i}{\partial x}, \quad (2.24a)$$

$$\chi_{z_0 z_0}^{(i)} = \frac{1}{2R(\theta)^2} \frac{\partial u_i}{\partial \theta} + \frac{1}{2R(\theta)} \frac{\partial v_i}{\partial x}, \quad \chi_{xz_0}^{(i)} = -\frac{1}{4R(\theta)} \frac{\partial^2 u_i}{\partial x \partial \theta} + \frac{1}{4} \frac{\partial^2 v_i}{\partial x^2}, \quad (2.24b)$$

$$\chi_{\theta z_0}^{(i)} = -\frac{1}{4R(\theta)^2} \frac{\partial^2 u_i}{\partial \theta^2} + \frac{1}{2R(\theta)} \frac{\partial w}{\partial x} + \frac{1}{4R(\theta)} \frac{\partial^2 v_i}{\partial x \partial \theta}, \quad (2.24c)$$

$$\begin{aligned} \chi_{x\theta_0}^{(i)} = & -\frac{1}{4R(\theta)^3} \left( \frac{dR(\theta)}{d\theta} \right) \frac{\partial w}{\partial \theta} + \frac{1}{4R(\theta)^3} \left( \frac{dR(\theta)}{d\theta} \right) v_i + \frac{1}{2R(\theta)^2} \frac{\partial^2 w}{\partial \theta^2} \\ & - \frac{1}{2R(\theta)^2} \frac{\partial v_i}{\partial \theta} - \frac{1}{2} \frac{\partial^2 w}{\partial x^2}, \end{aligned} \quad (2.24d)$$

$$\chi_{xx_1}^{(i)} = \frac{1}{2R(\theta)^2} \frac{\partial^2 w}{\partial x \partial \theta} - \frac{1}{2R(\theta)^2} \frac{\partial v_i}{\partial x}, \quad \chi_{\theta\theta_1}^{(i)} = \frac{1}{2R(\theta)^2} \frac{\partial v_i}{\partial x}, \quad (2.24e)$$

$$\chi_{zz_1}^{(i)} = -\frac{1}{2R(\theta)^2} \frac{\partial^2 w}{\partial x \partial \theta}, \quad \chi_{xz_1}^{(i)} = -\frac{1}{4R(\theta)^3} \frac{\partial w}{\partial \theta} + \frac{1}{4R(\theta)^3} v_i + \frac{1}{4R(\theta)} \frac{\partial^2 v_i}{\partial x^2}, \quad (2.24f)$$

$$\chi_{\theta z_1}^{(i)} = \frac{1}{4R(\theta)^3} \left( \frac{dR(\theta)}{d\theta} \right) \frac{\partial^2 w}{\partial x \partial \theta} - \frac{1}{4R(\theta)^3} \left( \frac{dR(\theta)}{d\theta} \right) \frac{\partial v_i}{\partial x} + \frac{1}{4R(\theta)^2} \frac{\partial^2 v_i}{\partial x \partial \theta}, \quad (2.24g)$$

$$\chi_{x\theta_1}^{(i)} = -\frac{1}{4R(\theta)^4} \left( \frac{dR(\theta)}{d\theta} \right) \frac{\partial w}{\partial \theta} + \frac{1}{4R(\theta)^4} \left( \frac{dR(\theta)}{d\theta} \right) v_i + \frac{1}{4R(\theta)^3} \frac{\partial^2 w}{\partial \theta^2} - \frac{1}{4R(\theta)^3} \frac{\partial v_i}{\partial \theta}, \quad (2.24h)$$

$$\chi_{xx_0}^{(2)} = -\frac{1}{2} \frac{\partial \psi_2}{\partial x} + \frac{1}{2R(\theta)} \frac{\partial^2 w}{\partial x \partial \theta} - \frac{1}{2R(\theta)} \frac{\partial v_2}{\partial x}, \quad (2.24i)$$

$$\chi_{\theta\theta_0}^{(2)} = \frac{1}{2R(\theta)} \frac{\partial \varphi_2}{\partial \theta} - \frac{1}{2R(\theta)^2} \frac{\partial u_2}{\partial \theta} - \frac{1}{2R(\theta)} \frac{\partial^2 w}{\partial x \partial \theta} + \frac{1}{2R(\theta)} \frac{\partial v_2}{\partial x}, \quad (2.24j)$$

$$\chi_{zz_0}^{(2)} = -\frac{1}{2R(\theta)} \frac{\partial \varphi_2}{\partial \theta} + \frac{1}{2R(\theta)^2} \frac{\partial u_2}{\partial \theta} + \frac{1}{2} \frac{\partial \psi_2}{\partial x}, \quad (2.24k)$$

$$\chi_{\theta z_0}^{(2)} = -\frac{1}{4R(\theta)^2} \frac{\partial^2 u_2}{\partial \theta^2} - \frac{\varphi_2}{4R(\theta)} + \frac{1}{4R(\theta)} \frac{\partial^2 v_2}{\partial x \partial \theta} + \frac{1}{4R(\theta)} \frac{\partial w}{\partial x}, \quad (2.24l)$$

$$\chi_{xz_0}^{(2)} = -\frac{1}{4R(\theta)^2} \frac{\partial w}{\partial \theta} - \frac{\psi_2}{4R(\theta)} + \frac{v_2}{4R(\theta)^2} - \frac{1}{4R(\theta)} \frac{\partial^2 u_2}{\partial x \partial \theta} + \frac{1}{4} \frac{\partial^2 v_2}{\partial x^2}, \quad (2.24m)$$

$$\chi_{x\theta_0}^{(2)} = -\frac{1}{4R(\theta)} \frac{\partial \psi_2}{\partial \theta} - \frac{1}{4R(\theta)^2} \frac{\partial v_2}{\partial \theta} + \frac{1}{4R(\theta)^2} \frac{\partial^2 w}{\partial \theta^2} + \frac{1}{4} \frac{\partial \varphi_2}{\partial x} - \frac{1}{4} \frac{\partial^2 w}{\partial x^2}, \quad (2.24n)$$

$$\chi_{xx_1}^{(2)} = -\frac{1}{2R(\theta)} \frac{\partial \psi_2}{\partial x}, \quad \chi_{\theta\theta_1}^{(2)} = -\frac{1}{2R(\theta)^2} \frac{\partial \varphi_2}{\partial \theta} + \frac{1}{2R(\theta)} \frac{\partial \psi_2}{\partial x}, \quad (2.24o)$$

$$\chi_{zz_1}^{(2)} = \frac{1}{2R(\theta)^2} \frac{\partial \varphi_2}{\partial \theta}, \quad \chi_{\theta z_1}^{(2)} = -\frac{1}{4R(\theta)^2} \frac{\partial^2 \varphi_2}{\partial \theta^2} + \frac{1}{4R(\theta)} \frac{\partial^2 \psi_2}{\partial x \partial \theta}, \quad (2.24p)$$

$$\chi_{xz_1}^{(2)} = \frac{1}{4R(\theta)^2} \psi_2 - \frac{1}{4R(\theta)} \frac{\partial^2 \varphi_2}{\partial x \partial \theta} + \frac{1}{4} \frac{\partial^2 \psi_2}{\partial x^2}, \quad \chi_{x\theta_1}^{(2)} = -\frac{1}{4R(\theta)^2} \frac{\partial \psi_2}{\partial \theta}. \quad (2.24q)$$

### 2.5 Hamilton’s principle

The Hamilton’s principle was employed to derive the equations of motion for the elliptical microshells. Based on this principle, the relation between the kinetic energy of the  $i$ th layer ( $T_i$ ) and the strain energy of the  $i$ th layer ( $U_i$ ) is stated as follows:

$$\int_{t_1}^{t_2} (\delta T_1 + \delta T_2 + \delta T_3 - \delta U_1 - \delta U_2 - \delta U_3) dt = 0. \tag{2.25}$$

Where  $\delta$  is the variational operator. The following equations are employed to calculate the kinetic energy and the strain energy variations:

$$\delta T_i = \int_{-\frac{h_i}{2}}^{\frac{h_i}{2}} \int_0^{2\pi} \int_0^L \rho_i \left\{ \dot{U}_i \delta \dot{U}_i + \dot{V}_i \delta \dot{V}_i + \dot{W}_i \delta \dot{W}_i \right\} R(\theta) dx d\theta dz_i, \quad i = 1, 2, 3, \tag{2.26a}$$

$$\delta T_i = \int_{-\frac{h_i}{2}}^{\frac{h_i}{2}} \int_0^{2\pi} \int_0^L \rho_i \left\{ \left( \dot{u}_i - z_i \frac{\partial \dot{w}}{\partial x} \right) \left( \delta \dot{u}_i - z_i \frac{\partial \delta \dot{w}}{\partial x} \right) + \left( \dot{v}_i - \frac{z_i}{R(\theta)} \frac{\partial \dot{w}}{\partial \theta} \right) \left( \delta \dot{v}_i - \frac{z_i}{R(\theta)} \frac{\partial \delta \dot{w}}{\partial \theta} \right) + \dot{w} \delta \dot{w} \right\} R(\theta) dx d\theta dz_i, \quad i = 1, 3, \tag{2.26b}$$

$$\delta T_2 = \int_{-\frac{h_2}{2}}^{\frac{h_2}{2}} \int_0^{2\pi} \int_0^L \rho_2 \left\{ \left( \dot{u}_2 + z_2 \dot{\phi}_2 \right) \left( \delta \dot{u}_2 + z_2 \delta \dot{\phi}_2 \right) + \left( \dot{v}_2 + z_2 \dot{\psi}_2 \right) \left( \delta \dot{v}_2 + z_2 \delta \dot{\psi}_2 \right) + \dot{w} \delta \dot{w} \right\} R(\theta) dx d\theta dz_2, \tag{2.26c}$$

and

$$\delta U_i = \int_{-\frac{h_i}{2}}^{\frac{h_i}{2}} \int_0^{2\pi} \int_0^L \left\{ \sigma_x^{(i)} \delta \varepsilon_x^{(i)} + \sigma_\theta^{(i)} \delta \varepsilon_\theta^{(i)} + \tau_{x\theta}^{(i)} \delta \gamma_{x\theta}^{(i)} + m_{xx}^{(i)} \delta \chi_{xx}^{(i)} + m_{\theta\theta}^{(i)} \delta \chi_{\theta\theta}^{(i)} + m_{zz}^{(i)} \delta \chi_{zz}^{(i)} + 2m_{x\theta}^{(i)} \delta \chi_{x\theta}^{(i)} + 2m_{xz}^{(i)} \delta \chi_{xz}^{(i)} + 2m_{\theta z}^{(i)} \delta \chi_{\theta z}^{(i)} \right\} R(\theta) dx d\theta dz_i, \tag{2.27a}$$

$$\delta U_i = \int_{-\frac{h_i}{2}}^{\frac{h_i}{2}} \int_0^{2\pi} \int_0^L \left\{ \sigma_{xx}^{(i)} \left( \delta \varepsilon_{xx0}^{(i)} + z_i \delta \varepsilon_{xx1}^{(i)} \right) + \sigma_{\theta\theta}^{(i)} \left( \delta \varepsilon_{\theta\theta0}^{(i)} + z_i \delta \varepsilon_{\theta\theta1}^{(i)} \right) + \tau_{x\theta}^{(i)} \left( \delta \gamma_{x\theta0}^{(i)} + z_i \delta \gamma_{x\theta1}^{(i)} \right) + m_{xx}^{(i)} \left( \delta \chi_{xx0}^{(i)} + z_i \delta \chi_{xx1}^{(i)} \right) + m_{\theta\theta}^{(i)} \left( \delta \chi_{\theta\theta0}^{(i)} + z_i \delta \chi_{\theta\theta1}^{(i)} \right) + m_{zz}^{(i)} \left( \delta \chi_{zz0}^{(i)} + z_i \delta \chi_{zz1}^{(i)} \right) + 2m_{x\theta}^{(i)} \left( \delta \chi_{x\theta0}^{(i)} + z_i \delta \chi_{x\theta1}^{(i)} \right) + 2m_{\theta z}^{(i)} \left( \delta \chi_{\theta z0}^{(i)} + z_i \delta \chi_{\theta z1}^{(i)} \right) + 2m_{xz}^{(i)} \left( \delta \chi_{xz0}^{(i)} + z_i \delta \chi_{xz1}^{(i)} \right) \right\} R(\theta) dx d\theta dz_i, \quad i = 1, 2, 3. \tag{2.27b}$$

For simplification, the elliptical microshell equations of motion were derived, using stress resultants and moment of mass inertia definitions in Eqs. (2.26) and (2.27) as follows:

$$N_{ij}^{(k)} = \int_{-\frac{h_k}{2}}^{\frac{h_k}{2}} \sigma_{ij}^{(k)} dz_k, \quad M_{ij}^{(k)} = \int_{-\frac{h_k}{2}}^{\frac{h_k}{2}} \sigma_{ij}^{(k)} z_k dz_k, \quad V_{iz}^{(k)} = \int_{-\frac{h_k}{2}}^{\frac{h_k}{2}} \tau_{iz}^{(k)} dz_k, \tag{2.28a}$$

$$G_{ij}^{(k)} = \int_{-\frac{h_k}{2}}^{\frac{h_k}{2}} m_{ij}^{(k)} dz_k, \quad H_{ij}^{(k)} = \int_{-\frac{h_k}{2}}^{\frac{h_k}{2}} m_{ij}^{(k)} z_k dz_k, \quad i, j = x, \theta, \quad k = 1, 2, 3, \quad (2.28b)$$

and

$$I_0^{(k)} = \int_{-\frac{h_k}{2}}^{\frac{h_k}{2}} \rho_k dz_k, \quad I_1^{(k)} = \int_{-\frac{h_k}{2}}^{\frac{h_k}{2}} \rho_k z_k dz_k, \quad I_2^{(k)} = \int_{-\frac{h_k}{2}}^{\frac{h_k}{2}} \rho_k z_k^2 dz_k, \quad k = 1, 2, 3, \quad (2.29)$$

Substituting Eqs. (2.28)-(2.29) into the Eqs. (2.26)-(2.27), the system’s kinetic and strain energies are obtained as follows:

$$\begin{aligned} \delta T_i = \int_0^L \int_0^{2\pi} \left\{ I_0^{(i)} \dot{u}_i \delta \dot{u}_i - I_1^{(i)} \dot{u}_i \frac{\partial \delta \dot{w}}{\partial x} - I_1^{(i)} \frac{\partial \dot{w}}{\partial x} \delta \dot{u}_i + I_2^{(i)} \frac{\partial \dot{w}}{\partial x} \frac{\partial \delta \dot{w}}{\partial x} + I_0^{(i)} \dot{v}_i \delta \dot{v}_i \right. \\ \left. - \frac{I_1^{(i)}}{R(\theta)} \dot{v} \frac{\partial \delta \dot{w}}{\partial \theta} - \frac{I_1^{(i)}}{R(\theta)} \frac{\partial \dot{w}}{\partial \theta} \delta \dot{v} + \frac{I_2^{(i)}}{R^2(\theta)} \frac{\partial \dot{w}}{\partial \theta} \frac{\partial \delta \dot{w}}{\partial \theta} + I_0^{(i)} \dot{w} \delta \dot{w} \right\} R(\theta) d\theta dx, \quad i = 1, 3, \quad (2.30a) \end{aligned}$$

$$\begin{aligned} \delta T_2 = \int_0^L \int_0^{2\pi} \left\{ I_0^{(2)} \dot{u}_2 \delta \dot{u}_2 + I_1^{(2)} \dot{u}_2 \delta \dot{\phi}_2 + I_1^{(2)} \dot{\phi}_2 \delta \dot{u}_2 + I_2^{(2)} \dot{\phi}_2 \delta \dot{\phi}_2 + I_0^{(2)} \dot{v}_2 \delta \dot{v}_2 + I_1^{(2)} \dot{v}_2 \delta \dot{\psi}_2 \right. \\ \left. + I_1^{(2)} \dot{\psi}_2 \delta \dot{v}_2 + I_2^{(2)} \dot{\psi}_2 \delta \dot{\psi}_2 + I_0^{(2)} \dot{w} \delta \dot{w} \right\} R(\theta) d\theta dx, \quad (2.30b) \end{aligned}$$

and

$$\begin{aligned} \delta U_i = \int_0^L \int_0^{2\pi} \left\{ N_x^{(i)} \delta \varepsilon_{xx0} + M_x^{(i)} \delta \varepsilon_{xx1} + N_\theta^{(i)} \delta \varepsilon_{\theta\theta 0} + M_\theta^{(i)} \delta \varepsilon_{\theta\theta 1} + N_{x\theta}^{(i)} \delta \gamma_{x\theta 0} + M_{x\theta}^{(i)} \delta \gamma_{x\theta 1} \right. \\ + G_{xx}^{(i)} \delta \chi_{xx0} + H_{xx}^{(i)} \delta \chi_{xx1} + G_{\theta\theta}^{(i)} \delta \chi_{\theta\theta 0} + H_{\theta\theta}^{(i)} \delta \chi_{\theta\theta 1} + G_{zz}^{(i)} \delta \chi_{zz 0} + H_{zz}^{(i)} \delta \chi_{zz 1} \\ + 2G_{x\theta}^{(i)} \delta \chi_{x\theta 0} + 2H_{x\theta}^{(i)} \delta \chi_{x\theta 1} + 2G_{\theta z}^{(i)} \delta \chi_{\theta z 0} + 2H_{\theta z}^{(i)} \delta \chi_{\theta z 1} + 2G_{xz}^{(i)} \delta \chi_{xz 0} \\ \left. + 2H_{xz}^{(i)} \delta \chi_{xz 1} \right\} R(\theta) d\theta dx, \quad i = 1, 2, 3. \quad (2.31) \end{aligned}$$

The equations of motion for the elliptical microshell were derived, utilizing Hamilton’s principle and integration by parts of Eqs. (2.30)-(2.31) as follows:

$$\begin{aligned} \frac{\partial N_x^{(1)}}{\partial x} + \frac{1}{R(\theta)} \frac{\partial N_{x\theta}^{(1)}}{\partial \theta} + \frac{1}{h_2} V_{xz}^{(2)} + \frac{R'(\theta)}{2R(\theta)^3} G_\theta^{(1)} - \frac{1}{2R(\theta)^2} \frac{\partial G_\theta^{(1)}}{\partial \theta} + \frac{1}{2R(\theta)^2} \frac{\partial G_z^{(1)}}{\partial \theta} - \frac{R'(\theta)}{2R(\theta)^3} G_z^{(1)} \\ + \frac{1}{2R(\theta)^2} \frac{\partial^2 G_{\theta z}^{(1)}}{\partial \theta^2} - \frac{R'(\theta)}{R(\theta)^3} \frac{\partial G_{\theta z}^{(1)}}{\partial \theta} + \frac{R'(\theta)^2}{R(\theta)^4} G_{\theta z}^{(1)} - \frac{R''(\theta)}{2R(\theta)^3} G_{\theta z}^{(1)} + \frac{1}{2R(\theta)} \frac{\partial^2 G_{xz}^{(1)}}{\partial x \partial \theta} + \frac{1}{4R(\theta)^2} \frac{\partial^2 G_{\theta z}^{(2)}}{\partial \theta^2} \\ - \frac{R'(\theta)}{2R(\theta)^3} \frac{\partial G_{\theta z}^{(2)}}{\partial \theta} + \frac{R'(\theta)^2}{2R(\theta)^4} G_{\theta z}^{(2)} - \frac{R''(\theta)}{4R(\theta)^3} G_{\theta z}^{(2)} - \frac{1}{2h_2 R(\theta)^2} \frac{\partial^2 H_{\theta z}^{(2)}}{\partial \theta^2} + \frac{R'(\theta)}{h_2 R(\theta)^3} \frac{\partial H_{\theta z}^{(2)}}{\partial \theta} \\ - \frac{R'(\theta)^2}{h_2 R(\theta)^4} H_{\theta z}^{(2)} + \frac{R''(\theta)}{2h_2 R(\theta)^3} H_{\theta z}^{(2)} - \frac{1}{2h_2 R(\theta)} G_{\theta z}^{(2)} + \frac{1}{4R(\theta)} \frac{\partial^2 G_{xz}^{(2)}}{\partial x \partial \theta} - \frac{1}{2h_2 R(\theta)} \frac{\partial^2 H_{xz}^{(2)}}{\partial x \partial \theta} \end{aligned}$$

$$\begin{aligned}
 &= I_0^{(1)} \frac{\partial^2 u_1}{\partial t^2} - I_1^{(1)} \frac{\partial^3 w}{\partial x \partial t^2} - \frac{I_0^{(2)} h_1}{8} \frac{\partial^3 w}{\partial x \partial t^2} - \frac{I_1^{(2)} \partial^2 u_1}{h_2 \partial t^2} - \frac{I_2^{(2)} h_1}{2h_2^2} \frac{\partial^3 w}{\partial x \partial t^2} - \frac{I_2^{(2)} h_3}{2h_2^2} \frac{\partial^3 w}{\partial x \partial t^2} \\
 &\quad + \frac{I_1^{(2)} h_1}{2h_2} \frac{\partial^3 w}{\partial x \partial t^2} + \frac{I_0^{(2)} \partial^2 u_1}{4 \partial t^2} - \frac{I_2^{(2)} \partial^2 u_1}{h_2^2 \partial t^2} + \frac{I_2^{(2)} \partial^2 u_3}{h_2^2 \partial t^2} + \frac{I_0^{(2)} h_3}{8} \frac{\partial^3 w}{\partial x \partial t^2} + \frac{I_0^{(2)} \partial^2 u_3}{4 \partial t^2}, \quad (2.32a)
 \end{aligned}$$

$$\begin{aligned}
 &\frac{\partial N_x^{(3)}}{\partial x} + \frac{1}{R(\theta)} \frac{\partial N_{x\theta}^{(3)}}{\partial \theta} - \frac{1}{h_2} V_{xz}^{(2)} + \frac{R'(\theta)}{2R(\theta)^3} G_\theta^{(3)} - \frac{1}{2R(\theta)^2} \frac{\partial G_\theta^{(3)}}{\partial \theta} + \frac{1}{2R(\theta)^2} \frac{\partial G_z^{(3)}}{\partial \theta} - \frac{R'(\theta)}{2R(\theta)^3} G_z^{(3)} \\
 &+ \frac{1}{2R(\theta)^2} \frac{\partial^2 G_{\theta z}^{(3)}}{\partial \theta^2} - \frac{R'(\theta)}{R(\theta)^3} \frac{\partial G_{\theta z}^{(3)}}{\partial \theta} + \frac{R'(\theta)^2}{R(\theta)^4} G_{\theta z}^{(3)} - \frac{R''(\theta)}{2R(\theta)^3} G_{\theta z}^{(3)} + \frac{1}{2R(\theta)} \frac{\partial^2 G_{xz}^{(3)}}{\partial x \partial \theta} + \frac{1}{4R(\theta)^2} \frac{\partial^2 G_{\theta z}^{(3)}}{\partial \theta^2} \\
 &- \frac{R'(\theta)}{2R(\theta)^3} \frac{\partial G_{\theta z}^{(2)}}{\partial \theta} + \frac{R'(\theta)^2}{2R(\theta)^4} G_{\theta z}^{(2)} - \frac{R''(\theta)}{4R(\theta)^3} G_{\theta z}^{(2)} + \frac{1}{2h_2 R(\theta)^2} \frac{\partial^2 H_{\theta z}^{(2)}}{\partial \theta^2} - \frac{R'(\theta)}{h_2 R(\theta)^3} \frac{\partial H_{\theta z}^{(2)}}{\partial \theta} \\
 &+ \frac{R'(\theta)^2}{h_2 R(\theta)^4} H_{\theta z}^{(2)} - \frac{R''(\theta)}{2h_2 R(\theta)^3} H_{\theta z}^{(2)} - \frac{1}{2h_2 R(\theta)} G_{\theta z}^{(2)} + \frac{1}{4R(\theta)} \frac{\partial^2 G_{xz}^{(2)}}{\partial x \partial \theta} + \frac{1}{2h_2 R(\theta)} \frac{\partial^2 H_{xz}^{(2)}}{\partial x \partial \theta} \\
 &= I_0^{(3)} \frac{\partial^2 u_3}{\partial t^2} - I_1^{(3)} \frac{\partial^3 w}{\partial x \partial t^2} - \frac{I_0^{(2)} h_1}{8} \frac{\partial^3 w}{\partial x \partial t^2} + \frac{I_1^{(2)} \partial^2 u_1}{h_2 \partial t^2} + \frac{I_2^{(2)} h_1}{2h_2^2} \frac{\partial^3 w}{\partial x \partial t^2} + \frac{I_2^{(2)} h_3}{2h_2^2} \frac{\partial^3 w}{\partial x \partial t^2} \\
 &\quad + \frac{I_1^{(2)} h_3}{2h_2} \frac{\partial^3 w}{\partial x \partial t^2} + \frac{I_0^{(2)} \partial^2 u_1}{4 \partial t^2} - \frac{I_2^{(2)} \partial^2 u_1}{h_2^2 \partial t^2} + \frac{I_2^{(2)} \partial^2 u_3}{h_2^2 \partial t^2} + \frac{I_0^{(2)} h_3}{8} \frac{\partial^3 w}{\partial x \partial t^2} + \frac{I_0^{(2)} \partial^2 u_3}{4 \partial t^2}, \quad (2.32b)
 \end{aligned}$$

$$\begin{aligned}
 &\frac{1}{R(\theta)} \frac{\partial N_\theta^{(1)}}{\partial \theta} + \frac{\partial N_{x\theta}^{(1)}}{\partial x} + \frac{1}{R(\theta)^2} \frac{\partial M_\theta^{(1)}}{\partial \theta} + \frac{1}{R(\theta)} \frac{\partial M_{x\theta}^{(1)}}{\partial x} + \frac{V_{\theta z}^{(2)}}{h_2} + \frac{1}{2R(\theta)} V_{\theta z}^{(2)} \\
 &- \frac{1}{2R(\theta)} \frac{\partial G_x^{(1)}}{\partial x} + \frac{1}{2R(\theta)} \frac{\partial G_\theta^{(1)}}{\partial x} - \frac{1}{2R(\theta)} \frac{\partial^2 G_{\theta z}^{(1)}}{\partial x \partial \theta} - \frac{1}{2} \frac{\partial^2 G_{xz}^{(1)}}{\partial x^2} - \frac{1}{2R(\theta)^2} G_{xz}^{(1)} - \frac{1}{2R(\theta)^2} \frac{\partial G_{x\theta}^{(1)}}{\partial \theta} \\
 &+ \frac{R'(\theta)}{2R(\theta)^3} G_{x\theta}^{(1)} - \frac{1}{4R(\theta)} \frac{\partial^2 G_{\theta z}^{(2)}}{\partial x \partial \theta} + \frac{1}{2h_2 R(\theta)} \frac{\partial^2 H_{\theta z}^{(2)}}{\partial x \partial \theta} - \frac{1}{4} \frac{\partial^2 G_{xz}^{(2)}}{\partial x^2} + \frac{1}{2h_2} \frac{\partial^2 H_{xz}^{(2)}}{\partial x^2} \\
 &- \frac{1}{2h_2 R(\theta)} G_{xz}^{(2)} - \frac{1}{4R(\theta)^2} G_{xz}^{(2)} + \frac{1}{2h_2 R(\theta)^2} H_{xz}^{(2)} \\
 &= I_0^{(1)} \frac{\partial^2 v_1}{\partial t^2} - \frac{I_1^{(1)} \partial^3 w}{R(\theta) \partial \theta \partial t^2} + \frac{h_1 I_1^{(2)} \partial^3 w}{2h_2 R(\theta) \partial \theta \partial t^2} - \frac{h_1 I_2^{(2)} \partial^3 w}{2h_2^2 R(\theta) \partial \theta \partial t^2} - \frac{h_3 I_2^{(2)} \partial^3 w}{2h_2^2 R(\theta) \partial \theta \partial t^2} - \frac{I_1^{(2)} \partial^2 v_1}{h_2 \partial t^2} \\
 &\quad - \frac{I_2^{(2)} \partial^2 v_3}{h_2^2 \partial t^2} + \frac{I_2^{(2)} \partial^2 v_1}{h_2^2 \partial t^2} + \frac{h_3 I_0^{(2)} \partial^3 w}{8R(\theta) \partial \theta \partial t^2} - \frac{h_1 I_0^{(2)} \partial^3 w}{8R(\theta) \partial \theta \partial t^2} + \frac{I_0^{(2)} \partial^2 v_1}{4 \partial t^2} + \frac{I_0^{(2)} \partial^2 v_3}{4 \partial t^2}, \quad (2.32c)
 \end{aligned}$$

$$\begin{aligned}
 &\frac{1}{R(\theta)} \frac{\partial N_\theta^{(3)}}{\partial \theta} + \frac{\partial N_{x\theta}^{(3)}}{\partial x} + \frac{1}{R(\theta)^2} \frac{\partial M_\theta^{(3)}}{\partial \theta} + \frac{1}{R(\theta)} \frac{\partial M_{x\theta}^{(3)}}{\partial x} - \frac{V_{\theta z}^{(2)}}{h_2} + \frac{1}{2R(\theta)} V_{\theta z}^{(2)} \\
 &- \frac{1}{2R(\theta)} \frac{\partial G_x^{(3)}}{\partial x} + \frac{1}{2R(\theta)} \frac{\partial G_\theta^{(3)}}{\partial x} - \frac{1}{2R(\theta)} \frac{\partial^2 G_{\theta z}^{(3)}}{\partial x \partial \theta} - \frac{1}{2} \frac{\partial^2 G_{xz}^{(3)}}{\partial x^2} - \frac{1}{2R(\theta)^2} G_{xz}^{(3)}
 \end{aligned}$$

$$\begin{aligned}
& -\frac{1}{2R(\theta)^2} \frac{\partial G_{x\theta}^{(3)}}{\partial \theta} + \frac{R'(\theta)}{2R(\theta)^3} G_{x\theta}^{(3)} - \frac{1}{4R(\theta)} \frac{\partial^2 G_{\theta z}^{(2)}}{\partial x \partial \theta} - \frac{1}{2h_2 R(\theta)} \frac{\partial^2 H_{\theta z}^{(2)}}{\partial x \partial \theta} \\
& - \frac{1}{4} \frac{\partial^2 G_{xz}^{(2)}}{\partial x^2} - \frac{1}{2h_2} \frac{\partial^2 H_{xz}^{(2)}}{\partial x^2} + \frac{1}{2h_2 R(\theta)} G_{xz}^{(2)} - \frac{1}{4R(\theta)^2} G_{xz}^{(2)} - \frac{1}{2h_2 R(\theta)^2} H_{xz}^{(2)} \\
& = I_0^{(3)} \frac{\partial^2 v_1}{\partial t^2} - \frac{I_1^{(3)}}{R(\theta)} \frac{\partial^3 w}{\partial \theta \partial t^2} + \frac{h_3 I_1^{(2)}}{2h_2 R(\theta)} \frac{\partial^3 w}{\partial \theta \partial t^2} + \frac{h_1 I_2^{(2)}}{2h_2^2 R(\theta)} \frac{\partial^3 w}{\partial \theta \partial t^2} + \frac{h_3 I_2^{(2)}}{2h_2^2 R(\theta)} \frac{\partial^3 w}{\partial \theta \partial t^2} + \frac{I_1^{(2)}}{h_2} \frac{\partial^2 v_3}{\partial t^2} \\
& \quad + \frac{I_2^{(2)}}{h_2^2} \frac{\partial^2 v_3}{\partial t^2} - \frac{I_2^{(2)}}{h_2^2} \frac{\partial^2 v_1}{\partial t^2} + \frac{h_3 I_0^{(2)}}{8R(\theta)} \frac{\partial^3 w}{\partial \theta \partial t^2} - \frac{h_1 I_0^{(2)}}{8R(\theta)} \frac{\partial^3 w}{\partial \theta \partial t^2} + \frac{I_0^{(2)}}{4} \frac{\partial^2 v_1}{\partial t^2} + \frac{I_0^{(2)}}{4} \frac{\partial^2 v_3}{\partial t^2}, \quad (2.32d) \\
& \frac{\partial^2 M_x^{(1)}}{\partial x^2} + \frac{\partial^2 M_x^{(3)}}{\partial x^2} + \frac{1}{R(\theta)^2} \frac{\partial^2 M_\theta^{(1)}}{\partial \theta^2} + \frac{1}{R(\theta)^2} \frac{\partial^2 M_\theta^{(3)}}{\partial \theta^2} - \frac{R'(\theta)}{R(\theta)^3} \frac{\partial M_\theta^{(1)}}{\partial \theta} - \frac{R'(\theta)}{R(\theta)^3} \frac{\partial M_\theta^{(3)}}{\partial \theta} \\
& \quad + \frac{2}{R(\theta)} \frac{\partial^2 M_{x\theta}^{(1)}}{\partial x \partial \theta} + \frac{2}{R(\theta)} \frac{\partial^2 M_{x\theta}^{(3)}}{\partial x \partial \theta} - \frac{N_\theta^{(1)}}{R(\theta)} - \frac{N_\theta^{(3)}}{R(\theta)} + \frac{\partial V_{xz}^{(2)}}{\partial x} + \frac{1}{R(\theta)} \frac{\partial V_{\theta z}^{(2)}}{\partial \theta} + \frac{h_1}{2h_2} \frac{\partial V_{xz}^{(2)}}{\partial x} \\
& \quad + \frac{h_3}{2h_2} \frac{\partial V_{xz}^{(2)}}{\partial x} + \frac{h_1}{2h_2 R(\theta)} \frac{\partial V_{\theta z}^{(2)}}{\partial \theta} + \frac{h_3}{2h_2 R(\theta)} \frac{\partial V_{\theta z}^{(2)}}{\partial \theta} + \frac{h_1}{4R(\theta)^2} \frac{\partial V_{\theta z}^{(2)}}{\partial \theta} - \frac{h_3}{4R(\theta)^2} \frac{\partial V_{\theta z}^{(2)}}{\partial \theta} \\
& \quad - \frac{h_1 R'(\theta)}{4R(\theta)^3} V_{\theta z}^{(2)} + \frac{h_3 R'(\theta)}{4R(\theta)^3} V_{\theta z}^{(2)} - \frac{1}{R(\theta)} \frac{\partial^2 G_x^{(1)}}{\partial x \partial \theta} - \frac{1}{R(\theta)} \frac{\partial^2 G_x^{(3)}}{\partial x \partial \theta} - \frac{R'(\theta)}{2R(\theta)^3} \frac{\partial H_z^{(1)}}{\partial x} \\
& \quad - \frac{R'(\theta)}{2R(\theta)^3} \frac{\partial H_z^{(3)}}{\partial x} + \frac{3R'(\theta)}{2R(\theta)^3} \frac{\partial G_{x\theta}^{(1)}}{\partial \theta} + \frac{3R'(\theta)}{2R(\theta)^3} \frac{\partial G_{x\theta}^{(3)}}{\partial \theta} + \frac{R'(\theta)}{R(\theta)^4} H_{xz}^{(1)} + \frac{R'(\theta)}{R(\theta)^4} H_{xz}^{(3)} \\
& \quad + \frac{1}{R(\theta)} \frac{\partial G_{\theta z}^{(1)}}{\partial x} + \frac{1}{R(\theta)} \frac{\partial G_{\theta z}^{(3)}}{\partial x} + \frac{\partial^2 G_{x\theta}^{(1)}}{\partial x^2} + \frac{\partial^2 G_{x\theta}^{(3)}}{\partial x^2} - \frac{1}{2R(\theta)} \frac{\partial^2 H_x^{(1)}}{\partial x \partial \theta} - \frac{1}{2R(\theta)} \frac{\partial^2 H_x^{(3)}}{\partial x \partial \theta} \\
& \quad - \frac{h_1}{4h_2 R(\theta)^2} \frac{\partial G_{xz}^{(2)}}{\partial \theta} - \frac{h_3}{4h_2 R(\theta)^2} \frac{\partial G_{xz}^{(2)}}{\partial \theta} + \frac{h_1 R'(\theta)}{4R(\theta)^4} G_{xz}^{(2)} - \frac{h_3 R'(\theta)}{4R(\theta)^4} G_{xz}^{(2)} + \frac{h_1}{4h_2 R(\theta)^3} \frac{\partial H_{xz}^{(2)}}{\partial \theta} \\
& \quad + \frac{h_3}{4h_2 R(\theta)^3} \frac{\partial H_{xz}^{(2)}}{\partial \theta} - \frac{1}{R(\theta)^2} \frac{\partial^2 G_{x\theta}^{(1)}}{\partial \theta^2} - \frac{1}{R(\theta)^2} \frac{\partial^2 G_{x\theta}^{(3)}}{\partial \theta^2} - \frac{1}{2R(\theta)^3} \frac{\partial^2 H_{x\theta}^{(1)}}{\partial \theta^2} - \frac{1}{2R(\theta)^3} \frac{\partial^2 H_{x\theta}^{(3)}}{\partial \theta^2} \\
& \quad + \frac{3R'(\theta)}{2R(\theta)^4} \frac{\partial H_{x\theta}^{(1)}}{\partial \theta} + \frac{3R'(\theta)}{2R(\theta)^4} \frac{\partial H_{x\theta}^{(3)}}{\partial \theta} + \frac{R''(\theta)}{2R(\theta)^3} G_{x\theta}^{(1)} + \frac{R''(\theta)}{2R(\theta)^3} G_{x\theta}^{(3)} + \frac{R''(\theta)}{2R(\theta)^4} H_{x\theta}^{(1)} + \frac{R''(\theta)}{2R(\theta)^4} H_{x\theta}^{(3)} \\
& \quad + \frac{1}{2R(\theta)^2} \frac{\partial^2 H_z^{(1)}}{\partial x \partial \theta} + \frac{1}{2R(\theta)^2} \frac{\partial^2 H_z^{(3)}}{\partial x \partial \theta} + \frac{h_1 R'(\theta)}{4h_2 R(\theta)^3} G_{xz}^{(2)} + \frac{h_3 R'(\theta)}{4h_2 R(\theta)^3} G_{xz}^{(2)} - \frac{h_1 R'(\theta)}{2h_2 R(\theta)^4} H_{xz}^{(2)} \\
& \quad - \frac{h_3 R'(\theta)}{2h_2 R(\theta)^4} H_{xz}^{(2)} - \frac{R'(\theta)^2}{R(\theta)^4} G_{x\theta}^{(1)} - \frac{R'(\theta)^2}{R(\theta)^4} G_{x\theta}^{(3)} - \frac{3R'(\theta)^2}{2R(\theta)^5} H_{x\theta}^{(1)} - \frac{3R'(\theta)^2}{2R(\theta)^5} H_{x\theta}^{(3)} - \frac{1}{2R(\theta)^3} \frac{\partial H_{xz}^{(1)}}{\partial \theta} \\
& \quad - \frac{1}{2R(\theta)^3} \frac{\partial H_{xz}^{(3)}}{\partial \theta} + \frac{1}{R(\theta)} \frac{\partial^2 G_\theta^{(1)}}{\partial x \partial \theta} + \frac{1}{R(\theta)} \frac{\partial^2 G_\theta^{(3)}}{\partial x \partial \theta} + \frac{R'(\theta)}{2R(\theta)^3} \frac{\partial H_x^{(1)}}{\partial x} + \frac{R'(\theta)}{2R(\theta)^3} \frac{\partial H_x^{(3)}}{\partial x} + \frac{R'(\theta)^2}{R(\theta)^4} \frac{\partial H_{\theta z}^{(1)}}{\partial x}
\end{aligned}$$

$$\begin{aligned}
 & + \frac{R'(\theta)^2}{R(\theta)^4} \frac{\partial H_{\theta z}^{(3)}}{\partial x} - \frac{R'(\theta)}{2R(\theta)^3} \frac{\partial^2 H_{\theta z}^{(1)}}{\partial x \partial \theta} - \frac{R'(\theta)}{2R(\theta)^3} \frac{\partial^2 H_{\theta z}^{(3)}}{\partial x \partial \theta} - \frac{R''(\theta)}{2R(\theta)^3} \frac{\partial H_{\theta z}^{(1)}}{\partial x} - \frac{R''(\theta)}{2R(\theta)^3} \frac{\partial H_{\theta z}^{(3)}}{\partial x} \\
 & - \frac{h_1}{8R(\theta)^3} \frac{\partial G_{xz}^{(2)}}{\partial \theta} + \frac{h_3}{8R(\theta)^3} \frac{\partial G_{xz}^{(2)}}{\partial \theta} - \frac{h_1}{4h_2R(\theta)} \frac{\partial G_{\theta z}^{(2)}}{\partial x} - \frac{h_3}{4h_2R(\theta)} \frac{\partial G_{\theta z}^{(2)}}{\partial x} \\
 = & I_0^{(1)} \frac{\partial^2 w}{\partial t^2} + I_0^{(2)} \frac{\partial^2 w}{\partial t^2} + I_0^{(3)} \frac{\partial^2 w}{\partial t^2} + \frac{I_1^{(1)}}{R(\theta)} \frac{\partial^3 v_1}{\partial \theta \partial t^2} + \frac{I_1^{(3)}}{R(\theta)} \frac{\partial^3 v_3}{\partial \theta \partial t^2} + \frac{I_0^{(2)} h_1}{8R(\theta)} \frac{\partial^3 v_1}{\partial \theta \partial t^2} - \frac{I_0^{(2)} h_3}{8R(\theta)} \frac{\partial^3 v_1}{\partial \theta \partial t^2} \\
 & + \frac{I_0^{(2)} h_1}{8R(\theta)} \frac{\partial^3 v_3}{\partial \theta \partial t^2} + \frac{I_0^{(2)} h_3}{8R(\theta)} \frac{\partial^3 v_3}{\partial \theta \partial t^2} - \frac{I_2^{(1)}}{R(\theta)^2} \frac{\partial^4 w}{\partial \theta^2 \partial t^2} - \frac{I_2^{(3)}}{R(\theta)^2} \frac{\partial^4 w}{\partial \theta^2 \partial t^2} + I_1^{(1)} \frac{\partial^3 u_1}{\partial x \partial t^2} + I_1^{(3)} \frac{\partial^3 u_3}{\partial x \partial t^2} \\
 & - I_2^{(1)} \frac{\partial^4 w}{\partial x^2 \partial t^2} - I_2^{(3)} \frac{\partial^4 w}{\partial x^2 \partial t^2} + \frac{I_0^{(2)} h_1}{8} \frac{\partial^3 u_1}{\partial x \partial t^2} - \frac{I_0^{(2)} h_3}{8} \frac{\partial^3 u_1}{\partial x \partial t^2} - \frac{I_0^{(2)} h_1}{8} \frac{\partial^3 u_3}{\partial x \partial t^2} - \frac{I_0^{(2)} h_3}{8} \frac{\partial^3 u_3}{\partial x \partial t^2} \\
 & + \frac{I_2^{(2)} h_1}{2R(\theta) h_2^2} \frac{\partial^3 v_1}{\partial \theta \partial t^2} + \frac{I_2^{(2)} h_3}{2R(\theta) h_2^2} \frac{\partial^3 v_1}{\partial \theta \partial t^2} - \frac{I_2^{(2)} h_1}{2R(\theta) h_2^2} \frac{\partial^3 v_3}{\partial \theta \partial t^2} - \frac{I_2^{(2)} h_3}{2R(\theta) h_2^2} \frac{\partial^3 v_3}{\partial \theta \partial t^2} - \frac{I_0^{(2)} h_1^2}{16} \frac{\partial^4 w}{\partial x^2 \partial t^2} \\
 & + \frac{I_0^{(2)} h_1 h_3}{8} \frac{\partial^4 w}{\partial x^2 \partial t^2} - \frac{I_0^{(2)} h_3^2}{16} \frac{\partial^4 w}{\partial x^2 \partial t^2} - \frac{I_2^{(2)} h_1^2}{4h_2^2} \frac{\partial^4 w}{\partial x^2 \partial t^2} - \frac{I_2^{(2)} h_1 h_3}{2h_2^2} \frac{\partial^4 w}{\partial x^2 \partial t^2} - \frac{I_2^{(2)} h_3^2}{4h_2^2} \frac{\partial^4 w}{\partial x^2 \partial t^2} \\
 & + \frac{I_1^{(2)} h_1^2}{4h_2} \frac{\partial^4 w}{\partial x^2 \partial t^2} - \frac{I_1^{(2)} h_3^2}{4h_2} \frac{\partial^4 w}{\partial x^2 \partial t^2} + \frac{I_2^{(2)} h_1^2 R'(\theta)}{4R(\theta)^3 h_2^2} \frac{\partial^3 w}{\partial \theta \partial t^2} + \frac{I_2^{(2)} h_1 h_3 R'(\theta)}{2R(\theta)^3 h_2^2} \frac{\partial^3 w}{\partial \theta \partial t^2} \\
 & + \frac{I_2^{(2)} h_3^2 R'(\theta)}{4R(\theta)^3 h_2^2} \frac{\partial^3 w}{\partial \theta \partial t^2}. \tag{2.32e}
 \end{aligned}$$

The Hooke's law in the mode of in-plane strain is expressed as follows:

$$\begin{Bmatrix} \sigma_{xx} \\ \sigma_{\theta\theta} \\ \sigma_{x\theta} \end{Bmatrix} = \begin{bmatrix} Q_{11}(z) & Q_{12}(z) & 0 \\ Q_{21}(z) & Q_{22}(z) & 0 \\ 0 & 0 & Q_{66}(z) \end{bmatrix} \begin{Bmatrix} \epsilon_{xx} \\ \epsilon_{\theta\theta} \\ \gamma_{x\theta} \end{Bmatrix}. \tag{2.33}$$

The couple stress tensor using the MCST is also expressed stated as:

$$m_{ij} = 2\mu(z) l^2 \chi_{ij}, \quad (i, j = x, \theta, z). \tag{2.34}$$

Where  $\mu$  is the shear modulus and  $l$  is the length scale parameter. To obtain stress results in term of displacements, the stiffness matrices are defined as follows:

$$[A_{ij}^{(k)}] = \int_{-\frac{h_k}{2}}^{\frac{h_k}{2}} [Q_{ij}^{(k)}(z)] dz_k, \quad [B_{ij}^{(k)}] = \int_{-\frac{h_k}{2}}^{\frac{h_k}{2}} [Q_{ij}^{(k)}(z)] z_k dz_k, \tag{2.35a}$$

$$[D_{ij}^{(k)}] = \int_{-\frac{h_k}{2}}^{\frac{h_k}{2}} [Q_{ij}^{(k)}(z)] z_k^2 dz_k, \quad k = 1, 2, 3, \tag{2.35b}$$

$$Y_0^{(k)} = \int_{-\frac{h_k}{2}}^{\frac{h_k}{2}} 2\mu_k(z) l^2 dz_k, \quad Y_1^{(k)} = \int_{-\frac{h_k}{2}}^{\frac{h_k}{2}} 2\mu_k(z) l^2 z_k dz_k, \tag{2.35c}$$

$$Y_2^{(k)} = \int_{-\frac{h_k}{2}}^{\frac{h_k}{2}} 2\mu_k(z) l^2 z_k^2 dz_k, \quad k=1,2,3. \quad (2.35d)$$

Where,  $A$ ,  $B$ , and  $D$  are tensile stiffness and flexural-tensile coupling stiffness and flexural stiffness matrices. By using Eqs. (2.28) and (2.35), the stress resultants of the microshell in terms of displacement are obtained as follows:

$$\begin{aligned} \{N_{ij}^{(k)}\} &= \int_{-\frac{h_k}{2}}^{\frac{h_k}{2}} \sigma_{ij}^{(k)} dz_k = \int_{-\frac{h_k}{2}}^{\frac{h_k}{2}} [Q_{ij}^{(k)}] \{\varepsilon_{ij}^{(k)}\} dz_k \\ &= \int_{-\frac{h_k}{2}}^{\frac{h_k}{2}} [Q_{ij}^{(k)}] \{\varepsilon_{ij_0}^{(k)} + z_k \varepsilon_{ij_1}^{(k)}\} dz_k = [A_{ij}^{(k)}] \{\varepsilon_{ij}^{(0)}\} + [B_{ij}^{(k)}] \{\varepsilon_{ij}^{(1)}\}, \end{aligned} \quad (2.36a)$$

$$\begin{aligned} \{M_{ij}^{(k)}\} &= \int_{-\frac{h_k}{2}}^{\frac{h_k}{2}} \sigma_{ij}^{(k)} z_k dz_k = \int_{-\frac{h_k}{2}}^{\frac{h_k}{2}} [Q_{ij}^{(k)}] \{\varepsilon_{ij}^{(k)}\} z_k dz_k \\ &= \int_{-\frac{h_k}{2}}^{\frac{h_k}{2}} [Q_{ij}^{(k)}] \{\varepsilon_{ij_0}^{(k)} + z_k \varepsilon_{ij_1}^{(k)}\} z_k dz_k = [B_{ij}^{(k)}] \{\varepsilon_{ij}^{(0)}\} + [D_{ij}^{(k)}] \{\varepsilon_{ij}^{(1)}\}, \end{aligned} \quad (2.36b)$$

$$\begin{aligned} \{V_{iz}^{(k)}\} &= \int_{-\frac{h_k}{2}}^{\frac{h_k}{2}} \tau_{iz}^{(k)} dz_k = \int_{-\frac{h_k}{2}}^{\frac{h_k}{2}} [Q_{ij}^{(k)}] \{\gamma_{iz}^{(k)}\} z_k dz_k \\ &= \int_{-\frac{h_k}{2}}^{\frac{h_k}{2}} [Q_{ij}^{(k)}] \{\gamma_{iz_0}^{(k)} + z_k \gamma_{iz_1}^{(k)}\} dz_k = [A_{ij}^{(k)}] \{\gamma_{iz}^{(0)}\} + [B_{ij}^{(k)}] \{\gamma_{iz}^{(1)}\}, \end{aligned} \quad (2.36c)$$

$$\begin{aligned} \{G_{ij}^{(k)}\} &= \int_{-\frac{h_k}{2}}^{\frac{h_k}{2}} m_{ij}^{(k)} dz_k = \int_{-\frac{h_k}{2}}^{\frac{h_k}{2}} 2\mu_k(z) l^2 \chi_{ij}^{(k)} dz_k \\ &= \int_{-\frac{h_k}{2}}^{\frac{h_k}{2}} 2\mu_k(z) l^2 \{\chi_{ij_0}^{(k)} + z_k \chi_{ij_1}^{(k)}\} dz_k = Y_0^{(k)} \chi_{ij_0}^{(k)} + Y_1^{(k)} \chi_{ij_1}^{(k)}, \end{aligned} \quad (2.36d)$$

$$\begin{aligned} \{H_{ij}^{(k)}\} &= \int_{-\frac{h_k}{2}}^{\frac{h_k}{2}} m_{ij}^{(k)} z_k dz_k = \int_{-\frac{h_k}{2}}^{\frac{h_k}{2}} 2\mu_k(z) l^2 \chi_{ij}^{(k)} z_k dz_k \\ &= \int_{-\frac{h_k}{2}}^{\frac{h_k}{2}} 2\mu_k(z) l^2 \{\chi_{ij_0}^{(k)} + z_k \chi_{ij_1}^{(k)}\} z_k dz_k = Y_1^{(k)} \chi_{ij_0}^{(k)} + Y_2^{(k)} \chi_{ij_1}^{(k)}, \\ &k = (1,2,3), \quad i, j = (x, \theta, z). \end{aligned} \quad (2.36e)$$

Substituting the stress resultants in Eq. (2.36) into the Eqs. (2.32a)-36, the equations of motion, in terms of displacement, are derived as follows:

$$L_{11}(u) + L_{12}(v) + L_{13}(w) = 0, \quad (2.37a)$$

$$L_{21}(u) + L_{22}(v) + L_{23}(w) = 0, \quad (2.37b)$$

$$L_{31}(u) + L_{32}(v) + L_{33}(w) = 0. \quad (2.37c)$$

Where  $L_{ij}$  are differential operators.

### 2.6 Geometrical parameters of the elliptical microshell

For the geometrical calculations, the elliptical cylindrical shell was considered as shown in Fig. 5.

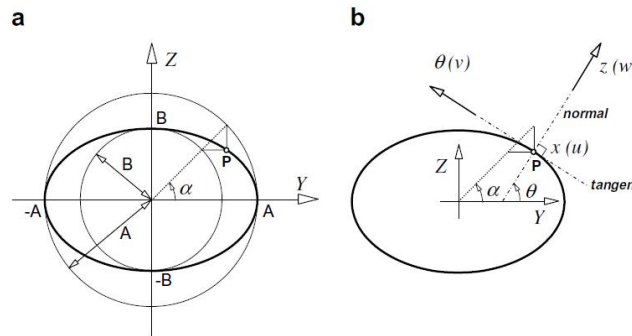


Figure 5: Geometrical parameters of elliptical cross-section.

The following parametric equations express the position of the point P:

$$Y = a \cos \alpha, \quad Z = b \sin \alpha. \tag{2.38}$$

Where A and B are sizes of the major and minor axes, and  $\alpha$  is the angle amount from the center of the ellipse. The purpose was to get the ellipse radius,  $R$ , and the ellipse's curvature,  $\chi$ , at any craved point on the ellipse, such as P. To calculate the radi and curvature of the ellipse, we use the tangent angle  $\theta$ , instead of central angle  $\alpha$ . This would represent the angle between the normal at the point P and the horizontal axis Y. The reason for choosing a tangential-vertical coordinate with  $\theta$  angle is that the displacement components  $V, W$  are in the tangential and vertical directions at point P on the ellipse. Also, the values of the ellipse radi and curvature are obtained as follows:

$$R(\alpha) = \frac{(a^2 \sin^2 \alpha + b^2 \cos^2 \alpha)^{\frac{3}{2}}}{ab}, \quad \chi(\alpha) = \frac{ab}{(a^2 \sin^2 \alpha + b^2 \cos^2 \alpha)^{\frac{3}{2}}} \tag{2.39}$$

Also,  $\alpha$  and  $\theta$  are inter-related as follows:

$$\alpha = \arctan \left( \frac{b}{a} \tan \theta \right). \tag{2.40}$$

Using Eqs. (2.39)-(2.40), the value of the ellipse radii is obtained at any desired point in terms of  $\theta$ . In most of previous papers, the value of the ellipse radii has been defined as follows [31]:

$$\frac{1}{R(s)} = 1 + \epsilon \cos(2s). \tag{2.41}$$

Where  $s$  is the dimensionless circumferential arc length  $0 \leq s \leq 2\pi$ , and also  $\varepsilon$  is the elliptical parameter of the microshell  $0 \leq \varepsilon \leq 1$ . The relation between the major vector  $a$  and minor vector  $b$  is stated as follows:

$$\varepsilon = 3Q - \frac{36}{35}Q^3, \quad Q = \frac{a-b}{a+b}. \quad (2.42)$$

## 2.7 Solution procedure

Circular cylindrical shells have infinite circular symmetric axes in the circumferential direction. The symmetric and anti-symmetric mode shapes are equal when the rotation of the cylinder is in the circumferential direction. However, for an elliptical cylindrical shell, there are only two symmetric axes, which are the same as the large and small radius of the ellipse, and the symmetric and anti-symmetric mode shapes are not equal. Consequently, it is crucial to analyze symmetric and anti-symmetric mode shapes in elliptical cylindrical shells.

The dual Fourier series can express elliptical cylindrical microshell displacements in the longitudinal and circumferential directions [31]. The displacements of the simply supported elliptical cylindrical shells for the symmetric mode can be stated as follows:

$$u^{sym}(x, \theta, t) = \sum_{m=0}^{\infty} \sum_{n=0}^{\infty} U_{mn} e^{i\omega t} \cos(n\theta) \cos\left(\frac{m\pi x}{L}\right), \quad (2.43a)$$

$$v^{sym}(x, \theta, t) = \sum_{m=0}^{\infty} \sum_{n=0}^{\infty} V_{mn} e^{i\omega t} \sin(n\theta) \sin\left(\frac{m\pi x}{L}\right), \quad (2.43b)$$

$$w^{sym}(x, \theta, t) = \sum_{m=0}^{\infty} \sum_{n=0}^{\infty} W_{mn} e^{i\omega t} \cos(n\theta) \sin\left(\frac{m\pi x}{L}\right). \quad (2.43c)$$

Where  $i^2 = -1$  and is the natural frequency. Also, the displacements of the elliptical cylindrical shells for the anti-symmetric mode shapes can be expressed as follows:

$$u^{Asym}(x, \theta, t) = \sum_{m=0}^{\infty} \sum_{n=1}^{\infty} U_{mn} e^{i\omega t} \sin(n\theta) \cos\left(\frac{m\pi x}{L}\right), \quad (2.44a)$$

$$v^{Asym}(x, \theta, t) = \sum_{m=1}^{\infty} \sum_{n=1}^{\infty} V_{mn} e^{i\omega t} \cos(n\theta) \sin\left(\frac{m\pi x}{L}\right), \quad (2.44b)$$

$$w^{Asym}(x, \theta, t) = \sum_{m=1}^{\infty} \sum_{n=1}^{\infty} W_{mn} e^{i\omega t} \sin(n\theta) \sin\left(\frac{m\pi x}{L}\right). \quad (2.44c)$$

Where  $U_{mn}$ ,  $V_{mn}$ ,  $W_{mn}$  are longitudinal, circumferential, and radial displacement domains, and  $m$  and  $n$  represent the longitudinal and circumferential wave numbers.

Substituting the displacement equations, Eqs. (2.43)-(2.45) into Eq. (2.37), the values of the symmetrical and asymmetrical weight residues are obtained as  $[res_i^{sym}(x, \theta, t), res_i^{Asym}(x, \theta, t)]$ .

We provide the number of the weighted residual equation later below. Then, the variable  $t$  is removed from the values of the weight residues by trigonometric simplification. Instead, the natural frequency value  $\omega$  is entered into the equations of the weight residues.

Applying the Galerkin's method on the entire domain of the elliptical shell, the frequency equations of the symmetrical and asymmetrical states are obtained as follows:

$$\int_0^{2\pi} \int_0^L res_1^{sym}(x,\theta) \cos(n\theta) \cos\left(\frac{m\pi x}{L}\right) dx d\theta = 0, \tag{2.45a}$$

$$\int_0^{2\pi} \int_0^L res_2^{sym}(x,\theta) \sin(n\theta) \sin\left(\frac{m\pi x}{L}\right) dx d\theta = 0, \tag{2.45b}$$

$$\int_0^{2\pi} \int_0^L res_3^{sym}(x,\theta) \cos(n\theta) \sin\left(\frac{m\pi x}{L}\right) dx d\theta = 0, \tag{2.45c}$$

$$\int_0^{2\pi} \int_0^L res_1^{Asym}(x,\theta) \sin(n\theta) \cos\left(\frac{m\pi x}{L}\right) dx d\theta = 0, \tag{2.45d}$$

$$\int_0^{2\pi} \int_0^L res_2^{Asym}(x,\theta) \cos(n\theta) \sin\left(\frac{m\pi x}{L}\right) dx d\theta = 0, \tag{2.45e}$$

$$\int_0^{2\pi} \int_0^L res_3^{Asym}(x,\theta) \sin(n\theta) \sin\left(\frac{m\pi x}{L}\right) dx d\theta = 0. \tag{2.45f}$$

The above-mentioned equations are applied to the problem of eigenvalues, which may be written in the following matrix form:

$$[K]\{X\} = (\omega^*)^2 [M]\{X\}. \tag{2.46}$$

In the above relation,  $\{X\} = \{U_{mn}, V_{mn}, W_{mn}\}^T$  is the displacement domain vector and  $\omega$  is the natural frequency of the microshell. Also,  $[M]$  is the mass matrix and  $[K]$  is the complex stiffness matrix. When equating the matrix determinants to zero, the natural frequencies and loss factors of the elliptical microshell are obtained as follows:

$$\omega = \sqrt{\text{Re}[(\omega^*)^2]}, \quad \eta = \frac{\text{Im}[(\omega^*)^2]}{\text{Re}[(\omega^*)^2]}. \tag{2.47}$$

### 3 Results and discussion

#### 3.1 Numerical results

The presented results consist of two parts: the first part is the validation of the solution, and the second part indicates the effects of the length scale parameter, porosity parameter, geometrical parameters of the microshell, longitudinal and circumferential wave number, and magnetic field intensity on the natural frequencies and damping ratios of the elliptical sandwich microshell with anMRF core.

### 3.2 Justification of the need for the current study

Based our extensive review of the relevant literature [4-47], no systematic analysis has been undertaken to date on the free vibration behavior of cylindrical, elliptical microshells. Thus, conducting the current study is justified as follows. Complex frequencies of an isotropic circular cylindrical shell in hinged boundary conditions are presented in Table 1. The results of the current study and those reported by Xiang, et al. [32] are in good agreement.

Table 1: The values of  $\omega^2 = \omega_0^2(1+i\eta)$  for three layered cylindrical shell.

$G_2 = 8.582 + i2.985, n = 0, L/R = 1, R/h = 300$ $\omega^2 = \omega_0^2(1+i\eta)$		
$m$	Present	Xiang [32]
1	2.4256E+09+i 2.0666E+05	2.4438E+09+i 2.0570E+05
2	2.4534E+09+i 1.9693E+06	2.4703E+09+i 1.9683E+06
3	2.4822E+09+i 5.3290E+06	2.4989E+09+i 5.3305E+06
4	2.5397E+09+i 1.0127E+06	2.5566E+09+i 1.0134E+07
5	2.6479E+09+i 1.6323E+06	2.6651E+09+i 1.6338E+07
6	2.8333E+09+i 2.3903E+07	2.8511E+09+i 2.3935E+07
7	3.1283E+09+i 3.2860E+07	3.1470E+09+i 3.2919E+07

Table 2: Dimensionless fundamental frequencies of isotropic circular cylindrical microshell in SS boundary condition.

$\Omega = \omega R \sqrt{\frac{\rho}{E}}, \frac{h}{R} = 0.02, \frac{L}{R} = 5, R = 2.32\text{nm}, \nu = 0.3$						
$(m,n)$	Theory	Present	Loy [15]	Error(%)	Ghadiri and Safarpour [27]	Error(%)
(1,1)	Classic( $l/h=0$ )	0.1954	0.1954	0%	0.1954	0%
	MCST( $l/h=1$ )	0.1955	0.1955	0%	0.1954	0.05%
(2,2)	Classic( $l/h=0$ )	0.2527	0.2532	0.19%	0.2527	0%
	MCST( $l/h=1$ )	0.2575	0.2575	0%	0.2573	0.07%
(3,3)	Classic( $l/h=0$ )	0.2758	0.2772	0.5%	0.2758	0%
	MCST( $l/h=1$ )	0.3101	0.3067	1.1%	0.3062	1.27%
(4,4)	Classic( $l/h=0$ )	0.3012	-	-	-	-
	MCST( $l/h=1$ )	0.4064	-	-	-	-
(5,5)	Classic( $l/h=0$ )	0.3422	-	-	-	-
	MCST( $l/h=1$ )	0.5588	-	-	-	-

In Tables 2 and 3, the dimensionless natural frequencies of an isotropic hinged circular cylindrical microshell of  $h/R = 0.02, 0.05$  are presented. There exists strong agreement between our results and those reported by Loy [15] and Ghadiri and Safarpour [27].

The dimensionless natural frequencies of the cross-section of an elliptical cylindrical shell are presented in Table 4. Of note, the boundary condition is hinged, and the results are based on various circumferential wave numbers. In this table, the strong agreement is evident between the results of the current study and those reported by three earlier

Table 3: Dimensionless fundamental frequencies of isotropic circular cylindrical microshell under SS boundary condition.

		$\Omega = \omega R \sqrt{\frac{\rho}{E}}, \frac{h}{R} = 0.05, \frac{l}{R} = 5, R = 2.32\text{nm}, \nu = 0.3$				
$(m, n)$	Theory	Present	Loy [15]	Error(%)	Ghadiri and Safarpour [27]	Error(%)
(1,1)	Classic( $l/h=0$ )	0.1954	0.1959	0.2%	0.1954	0%
	MCST( $l/h=1$ )	0.1962	0.1963	0.05%	0.1959	0.15%
(2,2)	Classic( $l/h=0$ )	0.2588	0.2623	1.3%	0.2588	0%
	MCST( $l/h=1$ )	0.2869	0.2869	0%	0.2854	0.5%
(3,3)	Classic( $l/h=0$ )	0.3144	0.3220	2.3%	0.3141	0%
	MCST( $l/h=1$ )	0.4620	0.4586	0.7%	0.4546	1.6%
(4,4)	Classic( $l/h=0$ )	0.4147	-	-	-	-
	MCST( $l/h=1$ )	0.7934	-	-	-	-
(5,5)	Classic( $l/h=0$ )	0.5714	-	-	-	-
	MCST( $l/h=1$ )	1.2339	-	-	-	-

Table 4: Dimensionless fundamental frequencies of isotropic elliptical cylindrical microshell under SS boundary condition.

		$\Omega = \omega R_0 \sqrt{\frac{\rho(1-\nu^2)}{E}}, \frac{h}{R_0} = 0.075, \frac{l}{R_0} = 6, m = 1, \nu = 0.25, \frac{a}{b} = 2.06$						
		Symmetric			Anti-symmetric			
$n$	Present	Soldatos [33]	Ahmed [34]	Ganapathi et al. [35]	Present	Soldatos [33]	Ahmed [34]	Ganapathi et al. [35]
1	0.06951	0.1595	0.06656	0.06643	0.07512	0.0808	0.08011	0.07996
2	0.15468	0.1702	0.15944	0.15897	0.09781	0.0931	0.09228	0.09264
3	0.16827	0.2779	0.16924	0.16958	0.15882	0.1608	0.16109	0.16037
4	0.29914	0.4796	0.29758	0.29434	0.29778	0.2996	0.30386	0.30023
5	0.48243	0.4845	0.49610	0.48643	0.32382	0.4839	0.31197	0.48588

one [33–35].

### 3.3 Parametric study

The free vibration analysis of the elliptical microshells with an MRF core was investigated in the current study by determining the natural frequencies and the corresponding loss factors for various circumferential wave numbers under simply supported boundary condition. The lowest magnitude of natural frequencies (the fundamental frequency) is reported in this section, which was highly critical to designing the shell’s structures. In this study, we chose porous materials, commonly known as steel foam, with the mechanical details established as  $E_0 = 210\text{MPa}$ ,  $\rho_0 = 7850\text{kg/m}^3$ . Also, due to the lack of experimental data on the elliptical microshells, the value of the length scale was considered as  $l = 15\mu\text{m}$ . Also, the experimental length scale has been considered as  $l = 17.6\mu\text{m}$ , based on the findings cited in [35]. In what follows,  $R_0$  is the equivalent radius of a circular cylindrical shell, with the circumference being equal to the parameter of the elliptical microshell. The parameter is calculated as follows:

$$R_0 = \frac{1}{2\pi} \int_0^{2\pi} \sqrt{r^2 + \left(\frac{dr}{d\theta}\right)^2} d\theta. \tag{3.1}$$

In what follows, the results are presented in two parts: single-layer elliptical microshell and 3-layer elliptical microshell.

### 3.4 Single-layer porous elliptical microshell

In part 1, the effect of various parameters, such as material length scale, porosity, geometry, longitudinal and circumferential wave number, and magnetic field intensity on the natural frequencies of the elliptical cylindrical microshells were investigated. The pattern of changes are illustrated in Figs. 6-10.

As shown in Fig. 6, by increasing the dimensionless material length scale ( $l/h$ ), the natural frequencies of the elliptical microshell, with  $n=1$ , are fairly constant. The natural frequency increases at  $n > 1$ , which is due to improvement in the shell's stiffness. Also, the effect of dimensionless material length scale on enhancing the natural frequency of the microshell is remarkable at higher circumferential wave numbers.

Fig. 7 shows the effect of length scale on the natural frequency of the elliptical microshells for various values of  $a/b$ . As noted, the dimensionless natural frequencies of the elliptical microshells increase by increases in the length scale parameter.

By increasing the elliptical ratio of  $a/b$ , the effect of the dimensionless length scale ( $l/h$ ) on increases in the natural frequency of the elliptical microshell becomes evident. In other words, the impact of the length scale on the natural frequency of the elliptical microshell is stronger at higher magnitudes of  $a/b$ .

Upon the free vibration analysis of circular cylindrical shells, the natural frequencies change at different circumferential wave numbers with similar trends. As shown in Fig. 8, it is noted that the variations of natural frequencies for elliptical shells are not the same at different circumferential wave numbers. As illustrated in Fig. 8 for  $n = 1$ , the

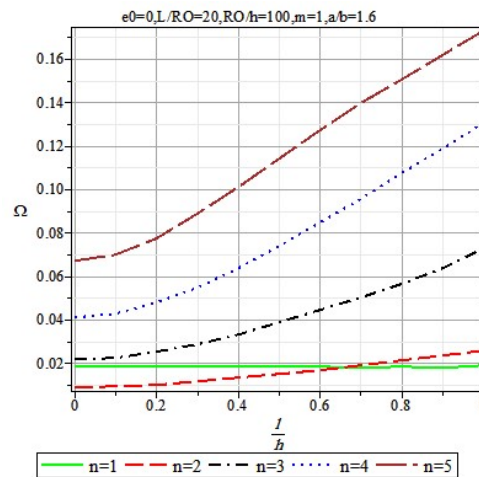


Figure 6: The dimensionless natural frequency of the elliptical microshell versus the length scale for various values of circumferential wave number in the symmetrical mode.

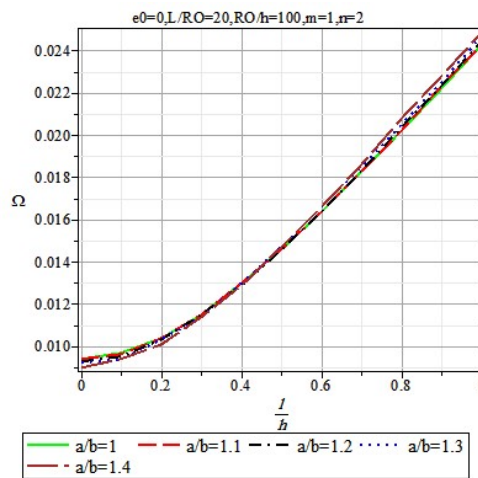


Figure 7: The dimensionless natural frequency of the elliptical microshell versus length scale for various magnitudes of  $a/b$  ratio in the symmetrical mode.

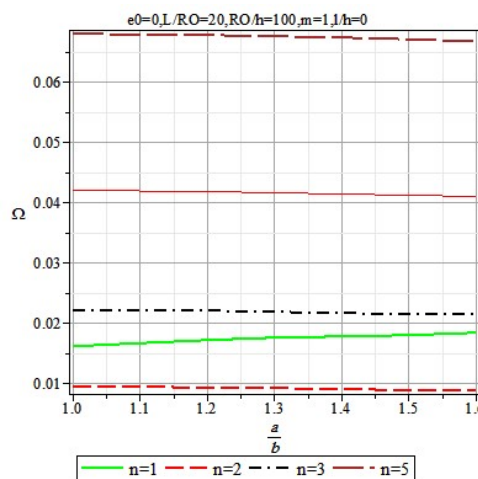


Figure 8: The dimensionless natural frequency of the elliptical microshell versus the  $a/b$  ratios for the various values of the circumferential wave numbers in symmetrical mode.

dimensionless natural frequency of the elliptical microshell increases by increasing  $a/b$  but for  $n > 1$ , the natural frequency declines as the  $a/b$  values rise.

Based on the data presented in Fig. 9, at  $n = 2$ , the value of the material length scale affects the trend of changes in the natural frequency of the elliptical microshell versus the values of  $a/b$  parameter. At low  $l/h$  values, changes in the natural frequency are lower than that of the  $a/b$  parameter. At higher  $l/h$  values, the trend of natural frequency changes for the elliptical microshell becomes more downward than that of the  $a/b$  parameter.

Table 5: The dimensionless natural frequency of the elliptical microshells for different aspect ratios, circumferential wave numbers and length scales in a symmetrical mode.

Symmetric		$\Omega = \omega R_0 \sqrt{\frac{\rho_0(1-v^2)}{E_0}}, e_0 = 0, \frac{L}{R_0} = 20, \frac{R_0}{h_1} = 100, m = 1, h_2 = 0$										
		$l/h=0$	$l/h=0.1$	$l/h=0.2$	$l/h=0.3$	$l/h=0.4$	$l/h=0.5$	$l/h=0.6$	$l/h=0.7$	$l/h=0.8$	$l/h=0.9$	$l/h=1$
$a/b=1$	$n=1$	0.0161	0.0161	0.0161	0.0161	0.0161	0.0161	0.0161	0.0161	0.0161	0.0161	0.0161
	$n=2$	0.0094	0.0097	0.0104	0.0115	0.0130	0.0146	0.0164	0.0183	0.0202	0.0222	0.0243
	$n=3$	0.0221	0.0230	0.0255	0.0292	0.0337	0.0387	0.0440	0.0496	0.0554	0.0612	0.0672
	$n=4$	0.0421	0.0438	0.0486	0.0557	0.0643	0.0740	0.0843	0.0950	0.1060	0.1173	0.1287
	$n=5$	0.0680	0.0708	0.0786	0.0900	0.1040	0.1196	0.1362	0.1536	0.1714	0.1896	0.2081
$a/b=1.1$	$n=1$	0.0166	0.0166	0.0166	0.0166	0.0166	0.0166	0.0166	0.0166	0.0166	0.0166	0.0167
	$n=2$	0.0094	0.0096	0.0104	0.0115	0.0130	0.0146	0.0164	0.0183	0.0202	0.0223	0.0243
	$n=3$	0.0221	0.0230	0.0255	0.0291	0.0336	0.0386	0.0440	0.0496	0.0553	0.0612	0.0671
	$n=4$	0.0420	0.0438	0.0486	0.0557	0.0643	0.0739	0.0842	0.0949	0.1060	0.1172	0.1286
	$n=5$	0.0679	0.0707	0.0785	0.0900	0.1040	0.1195	0.1362	0.1535	0.1713	0.1895	0.2080
$a/b=1.2$	$n=1$	0.0171	0.0171	0.0171	0.0171	0.0171	0.0171	0.0171	0.0171	0.0171	0.0171	0.0171
	$n=2$	0.0093	0.0095	0.0103	0.0115	0.0129	0.0146	0.0164	0.0183	0.0204	0.0223	0.0245
	$n=3$	0.0220	0.0229	0.0254	0.0290	0.0335	0.0385	0.0439	0.0494	0.0552	0.0611	0.0670
	$n=4$	0.0419	0.0436	0.0484	0.0555	0.0642	0.0738	0.0840	0.0948	0.1058	0.1170	0.1284
	$n=5$	0.0678	0.0706	0.0784	0.0899	0.1038	0.1194	0.1360	0.1533	0.1712	0.1893	0.2078
$a/b=1.3$	$n=1$	0.0175	0.0175	0.0175	0.0175	0.0175	0.0175	0.0175	0.0175	0.0175	0.0175	0.0175
	$n=2$	0.0092	0.0094	0.0103	0.0114	0.0130	0.0147	0.0166	0.0185	0.0205	0.0225	0.0247
	$n=3$	0.0218	0.0227	0.0253	0.0289	0.0334	0.0384	0.0438	0.0494	0.0551	0.0610	0.0669
	$n=4$	0.0417	0.0435	0.0483	0.0554	0.0640	0.0736	0.0839	0.0946	0.1056	0.1168	0.1281
	$n=5$	0.0676	0.0704	0.0782	0.0896	0.1036	0.1191	0.1357	0.1530	0.1708	0.1878	0.2075
$a/b=1.4$	$n=1$	0.0178	0.0178	0.0178	0.0178	0.0178	0.0178	0.0178	0.0178	0.0181	0.0176	0.0172
	$n=2$	0.0090	0.0094	0.0101	0.0114	0.0129	0.0147	0.0166	0.0186	0.0208	0.0228	0.0249
	$n=3$	0.0217	0.0226	0.0251	0.0288	0.0333	0.0383	0.0437	0.0493	0.0551	0.0609	0.0669
	$n=4$	0.0415	0.0433	0.0481	0.0551	0.0638	0.0734	0.0836	0.0943	0.1053	0.1165	0.1279
	$n=5$	0.0674	0.0702	0.0779	0.0894	0.1033	0.1188	0.1353	0.1524	0.1699	0.1873	0.2014
$a/b=1.5$	$n=1$	0.0180	0.0180	0.0181	0.0180	0.0180	0.0180	0.0179	0.0181	0.0182	0.0189	0.0182
	$n=2$	0.0089	0.0091	0.0101	0.0114	0.0130	0.0147	0.0165	0.0187	0.0208	0.0231	0.0253
	$n=3$	0.0215	0.0224	0.0250	0.0287	0.0332	0.0383	0.0436	0.0493	0.0552	0.0613	0.0679
	$n=4$	0.0413	0.0430	0.0478	0.0549	0.0636	0.0732	0.0835	0.0942	0.1053	0.1165	0.1280
	$n=5$	0.0671	0.0699	0.0777	0.0890	0.1027	0.1178	0.1336	0.1498	0.1658	0.1806	0.1906
$a/b=1.6$	$n=1$	0.0183	0.0183	0.0183	0.0183	0.0184	0.0183	0.0184	0.0180	0.0183	0.0177	0.0190
	$n=2$	0.0088	0.0091	0.0100	0.0113	0.0130	0.0147	0.0168	0.0187	0.0209	0.0232	0.0256
	$n=3$	0.0214	0.0223	0.0248	0.0286	0.0332	0.0384	0.0441	0.0500	0.0564	0.0635	0.0728
	$n=4$	0.0410	0.0428	0.0476	0.0548	0.0637	0.0736	0.0843	0.0954	0.1069	0.1186	0.1305
	$n=5$	0.0668	0.0696	0.0773	0.0883	0.1010	0.1142	0.1272	0.1395	0.1500	0.1615	0.1730

In the classical theory ( $l/h=0$ ), by increasing the circumferential wave number from  $n = 1$  to  $n = 2$ , the natural frequency of the elliptical microshells decreases, and for  $n > 1$ , the natural frequency increases (Fig. 10). Although in the MCST, at large values of the material length scale the dimensionless natural frequency of the elliptical microshell increases when the circumferential wave number increases.

Table 6 presents the natural frequency values for the elliptical microshell at different values of the  $a/b$ , the circumferential wave numbers, and the porosity in a symmetrical mode. The corresponding diagrams are illustrated in Figs. 11-14.

Based on the data presented in Fig. 11, it is noted that by increasing the porosity values ( $e_0$ ), the dimensionless natural frequency of the elliptical microshells is almost constant for  $n = 1$  and grows when  $n > 1$ . As the porosity values increase, both the stiffness and inertia of the microshell drop. However, a decline in the inertia is more significant than that of the stiffness, which leads to increases in the natural frequency of the microshell. Fig. 11 also shows that the effect of porosity parameter is stronger at higher circumferential wave numbers.

Table 6: The dimensionless natural frequency values of the elliptical microshell for various values of the elliptical ratios, circumferential wave numbers and porosity in a symmetrical mode.

Symmetric		$\Omega = \omega R_0 \sqrt{\frac{\rho_0(1-\nu^2)}{E_0}}, \frac{l}{h} = 0, \frac{L}{R_0} = 20, \frac{R_0}{h_1} = 100, m = 1, h_2 = 0, \text{dist type1}$										
		$e_0=0$	$e_0=0.1$	$e_0=0.2$	$e_0=0.3$	$e_0=0.4$	$e_0=0.5$	$e_0=0.6$	$e_0=0.7$	$e_0=0.8$	$e_0=0.9$	$e_0=1$
$a/b=1$	$n=1$	0.0161	0.0161	0.0161	0.0161	0.0161	0.0161	0.0161	0.0161	0.0161	0.0161	0.0161
	$n=2$	0.0094	0.0095	0.0096	0.0097	0.0099	0.0100	0.0102	0.0105	0.0107	0.0111	0.0116
	$n=3$	0.0221	0.0224	0.0228	0.0232	0.0237	0.0242	0.0248	0.0256	0.0265	0.0277	0.0292
	$n=4$	0.0421	0.0427	0.0434	0.0442	0.0451	0.0461	0.0474	0.0488	0.0506	0.0529	0.0558
	$n=5$	0.0680	0.0690	0.0701	0.0714	0.0728	0.0745	0.0765	0.0789	0.0818	0.0854	0.0901
$a/b=1.25$	$n=1$	0.0173	0.0173	0.0173	0.0173	0.0173	0.0173	0.0173	0.0173	0.0173	0.0173	0.0173
	$n=2$	0.0092	0.0093	0.0094	0.0096	0.0097	0.0099	0.0101	0.0103	0.0106	0.0109	0.0114
	$n=3$	0.0219	0.0222	0.0226	0.0230	0.0235	0.0240	0.0246	0.0254	0.0263	0.0275	0.0290
	$n=4$	0.0418	0.0424	0.0431	0.0439	0.0448	0.0459	0.0471	0.0485	0.0503	0.0526	0.0554
	$n=5$	0.0677	0.0687	0.0698	0.0711	0.0725	0.0742	0.0762	0.0786	0.0815	0.0851	0.0897
$a/b=1.5$	$n=1$	0.0181	0.0181	0.0181	0.0181	0.0181	0.0181	0.0181	0.0181	0.0181	0.0181	0.0181
	$n=2$	0.0089	0.0090	0.0091	0.0092	0.0094	0.0095	0.0097	0.0100	0.0102	0.0106	0.0111
	$n=3$	0.0215	0.0218	0.0222	0.0226	0.0230	0.0236	0.0242	0.0249	0.0258	0.0270	0.0284
	$n=4$	0.0413	0.0419	0.0426	0.0433	0.0442	0.0453	0.0465	0.0479	0.0497	0.0519	0.0547
	$n=5$	0.0671	0.0681	0.0692	0.0705	0.0719	0.0736	0.0755	0.0779	0.0808	0.0843	0.0889
$a/b=1.75$	$n=1$	0.0185	0.0186	0.0186	0.0186	0.0186	0.0186	0.0186	0.0186	0.0186	0.0186	0.0186
	$n=2$	0.0086	0.0087	0.0088	0.0089	0.0090	0.0092	0.0094	0.0096	0.0099	0.0103	0.0107
	$n=3$	0.0211	0.0214	0.0218	0.0221	0.0226	0.0231	0.0237	0.0244	0.0253	0.0264	0.0278
	$n=4$	0.0406	0.0412	0.0418	0.0426	0.0435	0.0445	0.0457	0.0471	0.0488	0.0510	0.0538
	$n=5$	0.0664	0.0674	0.0685	0.0697	0.0711	0.0728	0.0747	0.0770	0.0798	0.0834	0.0879
$a/b=2$	$n=1$	0.0189	0.0189	0.0189	0.0189	0.0190	0.0190	0.0190	0.0190	0.0190	0.0190	0.0190
	$n=2$	0.0084	0.0085	0.0086	0.0087	0.0088	0.0089	0.0091	0.0093	0.0096	0.0100	0.0104
	$n=3$	0.0207	0.0210	0.0213	0.0216	0.0221	0.0226	0.0232	0.0239	0.0247	0.0258	0.0272
	$n=4$	0.0376	0.0386	0.0396	0.0406	0.0417	0.0429	0.0443	0.0458	0.0476	0.0499	0.0527
	$n=5$	0.0662	0.0671	0.0682	0.0694	0.0708	0.0724	0.0743	0.0766	0.0793	0.0827	0.0872

From the data presented in Fig. 12, it may be concluded that for all values of  $a/b$ , the natural frequencies of the microshell increase if the porosity increases. Also, Fig. 13 provides additional support for that conclusion, which is similar to those discussed for

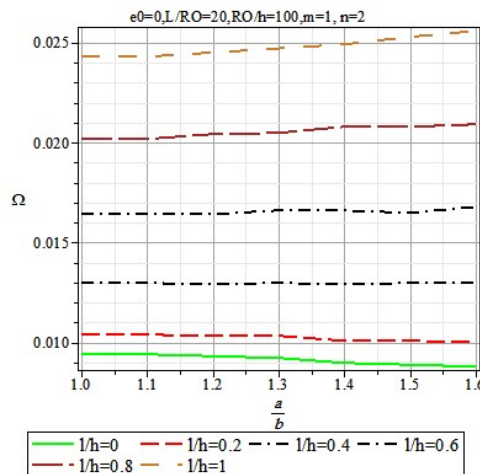


Figure 9: The dimensionless natural frequency of the elliptical microshells versus  $a/b$  for different length scale values in a symmetrical mode.

Table 7: The dimensionless natural frequency of porous elliptical cylindrical microshells for different values of  $L/R_0$ , circumferential wave numbers and  $R_0/h$  in a symmetrical mode.

Symmetric		$\Omega = \omega R_0 \sqrt{\frac{\rho_0(1-\nu^2)}{E_0}}, \frac{l}{h} = 0.2, m = 1, e_0 = 1, \frac{a}{b} = 1.3, h_2 = 0, \text{dist type1}$			
		$R_0/h_1 = 10$	$R_0/h_1 = 20$	$R_0/h_1 = 50$	$R_0/h_1 = 100$
$L/R_0 = 5$	$n = 1$	0.2029	0.2021	0.2019	0.2017
	$n = 2$	0.1386	0.0943	0.0760	0.0755
	$n = 3$	0.2973	0.1650	0.0743	0.0486
	$n = 4$	0.5148	0.3050	0.1252	0.0633
	$n = 5$	0.8719	0.4871	0.1979	0.1002
$L/R_0 = 10$	$n = 1$	0.0539	0.0641	0.0641	0.0641
	$n = 2$	0.1079	0.0599	0.0299	0.0226
	$n = 3$	0.2947	0.1574	0.0627	0.0329
	$n = 4$	0.6143	0.2982	0.1212	0.0609
	$n = 5$	0.6262	0.4823	0.1956	0.0981
$L/R_0 = 20$	$n = 1$	0.0074	0.0175	0.0175	0.0175
	$n = 2$	0.1076	0.0560	0.0229	0.0122
	$n = 3$	0.2753	0.1561	0.0628	0.0315
	$n = 4$	0.5108	0.2985	0.1206	0.0604
	$n = 5$	0.5971	0.4811	0.1951	0.0978

Fig. 8.

As shown in Fig. 14, by increasing the values of  $a/b$ , the dimensionless natural frequencies of the elliptical microshell increase for  $n = 1$  and decrease for  $n > 1$ . However, the effect of variations in the porosity values is negligible for  $n = 1$ .

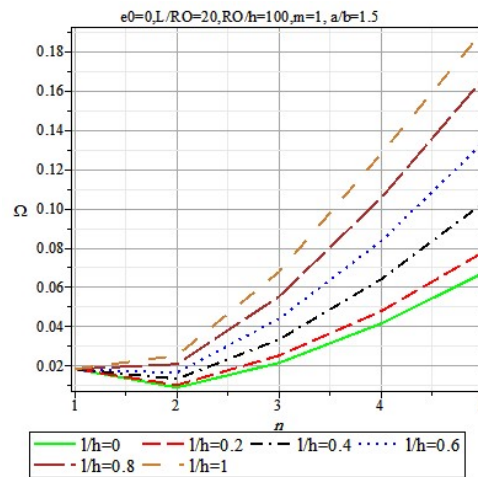


Figure 10: The dimensionless natural frequency of the elliptical microshell versus the circumferential wave number for various values of the length scale in a symmetrical mode.

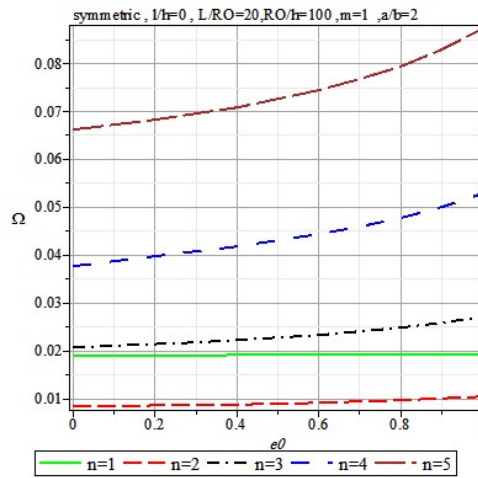


Figure 11: The dimensionless natural frequency values of the elliptical microshell versus the circumferential wave numbers at different length scale values in a symmetrical mode.

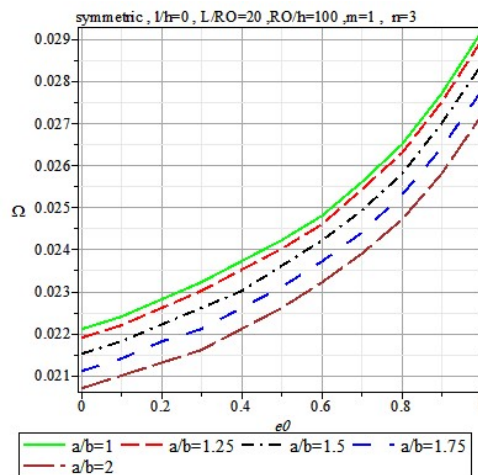


Figure 12: The dimensionless natural frequency of the elliptical microshell versus the circumferential wave numbers for various length scale values in a symmetrical mode.

Table 7 presents the dimensionless natural frequency for different values of  $l/R_0$ , circumferential wave numbers and  $R_0/h$  in a symmetrical mode. The corresponding diagrams are illustrated in Fig. 15. By increasing the  $R_0/h$  at  $n = 1$ , the dimensionless natural frequency of the elliptical microshell is fairly constant. However, for  $n > 1$ , these values decrease, which arise from a decrease in the structure's stiffness.

Table 8 reflects the dimensionless natural frequency of the elliptical microshell for various values of  $a/b$ , circumferential wave numbers, and the porosity parameters in symmetric and asymmetrical modes, with the corresponding diagrams shown in Figs. 16-

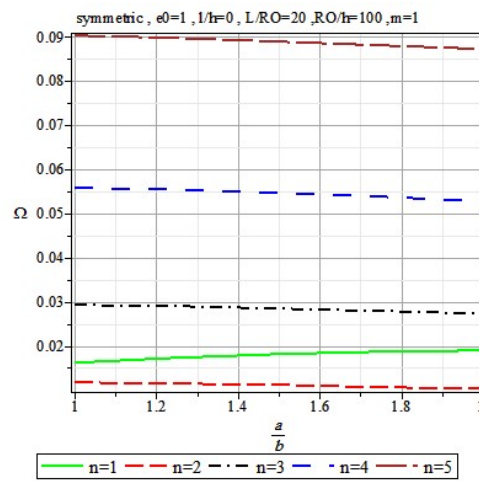


Figure 13: The dimensionless natural frequency of the elliptical microshell versus circumferential wave numbers for different values of the length scale in a symmetrical mode.

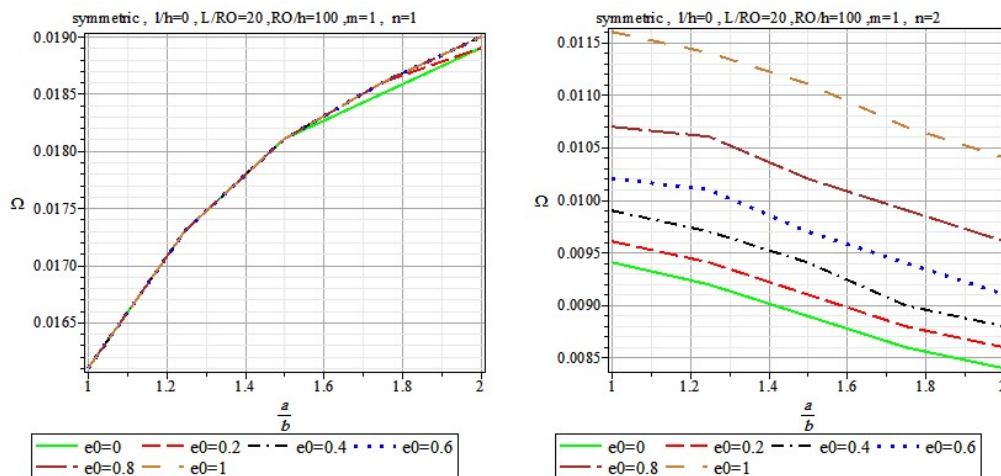


Figure 14: The dimensionless natural frequency of the elliptical microshells versus the circumferential wave numbers for different values of the length scale in a symmetrical mode.

18.

Fig. 16 shows that by increasing the porosity parameters, in the symmetrical mode for  $n = 1$  and asymmetrical mode for  $n = 2$ , the dimensionless natural frequencies of the elliptical microshell are fairly constant; however, for other cases it is increasing. Besides, the circumferential wave numbers for  $n = 1$  or 3 for a symmetrical mode, the natural frequencies of the elliptical microshell are more than the corresponding values for the asymmetrical mode. The situation is the opposite if  $n = 2$ . Also, by increasing the circumferential wave numbers, the differences between the symmetrical and asymmetrical

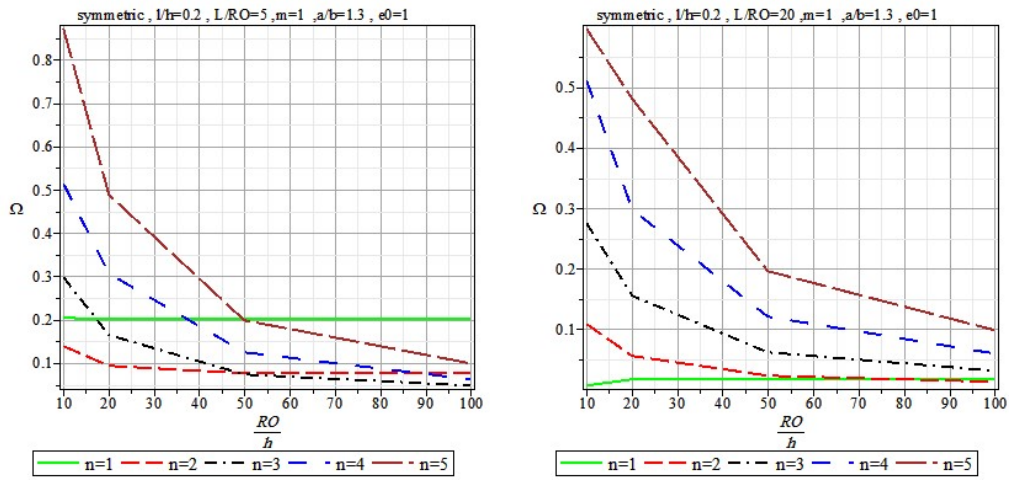


Figure 15: The dimensionless natural frequency of the elliptical microshells versus  $R_0/h$  at various values of circumferential wave numbers in a symmetrical mode.

Table 8: The dimensionless natural frequency of the elliptical microshell for various values of  $a/b$ , circumferential wave numbers and porosity parameters in symmetrical and asymmetrical modes.

		$\Omega = \omega R_0 \sqrt{\frac{\rho_0(1-\nu^2)}{E_0}}, \frac{l}{h} = 0.2, \frac{L}{R_0} = 20, \frac{R_0}{h_1} = 100, m = 1, h_2 = 0, \text{dist type1}$									
		$e_0 = 0$		$e_0 = 0.25$		$e_0 = 0.5$		$e_0 = 0.75$		$e_0 = 1$	
		sym	asym	sym	asym	sym	asym	sym	asym	Sym	asym
$a/b = 1$	$n = 1$	0.0161	0.0161	0.0161	0.0161	0.0161	0.0161	0.0161	0.0161	0.0161	0.0161
	$n = 2$	0.0104	0.0104	0.0106	0.0106	0.0110	0.0110	0.0115	0.0115	0.0124	0.0124
	$n = 3$	0.0255	0.0255	0.0263	0.0263	0.0273	0.0273	0.0290	0.0290	0.0318	0.0318
	$n = 4$	0.0486	0.0486	0.0501	0.0501	0.0522	0.0522	0.0553	0.0553	0.0608	0.0608
	$n = 5$	0.0786	0.0786	0.0809	0.0809	0.0843	0.0843	0.0894	0.0894	0.0983	0.0983
$a/b = 1.25$	$n = 1$	0.0173	0.0103	0.0173	0.0105	0.0173	0.0109	0.0173	0.0114	0.0173	0.0123
	$n = 2$	0.0103	0.0147	0.0105	0.0147	0.0109	0.0147	0.0114	0.0147	0.0123	0.0147
	$n = 3$	0.0253	0.0253	0.0261	0.0260	0.0271	0.0271	0.0288	0.0287	0.0316	0.0316
	$n = 4$	0.0484	0.0484	0.0498	0.0498	0.0519	0.0519	0.0550	0.0550	0.0605	0.0605
	$n = 5$	0.0783	0.0783	0.0806	0.0806	0.0840	0.0840	0.0891	0.0891	0.0979	0.0930
$a/b = 1.5$	$n = 1$	0.0181	0.0101	0.0181	0.0103	0.0181	0.0107	0.0181	0.0112	0.0181	0.0121
	$n = 2$	0.0101	0.0134	0.0103	0.0134	0.0106	0.0134	0.0111	0.0134	0.0120	0.0134
	$n = 3$	0.0250	0.0249	0.0257	0.0256	0.0267	0.0267	0.0283	0.0283	0.0311	0.0310
	$n = 4$	0.0478	0.0478	0.0493	0.0493	0.0513	0.0513	0.0544	0.0544	0.0598	0.0598
	$n = 5$	0.0777	0.0777	0.0800	0.0800	0.0833	0.0833	0.0883	0.0884	0.0971	0.0930
$a/b = 1.75$	$n = 1$	0.0186	0.0099	0.0186	0.0101	0.0186	0.0104	0.0187	0.0110	0.0187	0.0119
	$n = 2$	0.0098	0.0123	0.0101	0.0123	0.0104	0.0123	0.0109	0.0123	0.0118	0.0123
	$n = 3$	0.0246	0.0244	0.0253	0.0251	0.0263	0.0261	0.0279	0.0277	0.0306	0.0304
	$n = 4$	0.0477	0.0477	0.0491	0.0492	0.0510	0.0512	0.0541	0.0543	0.0594	0.0597
	$n = 5$	0.0770	0.0769	0.0792	0.0792	0.0823	0.0824	0.0870	0.0874	0.0952	0.0932

results decline.

As seen in Fig. 17, the dimensionless natural frequencies increase for all values of  $a/b$ , due to increases in the porosity values. Also, as the circumferential wave number ( $n = 3$ ) is an odd value, for all values of  $a/b$ , the values of the natural frequency of the microshell

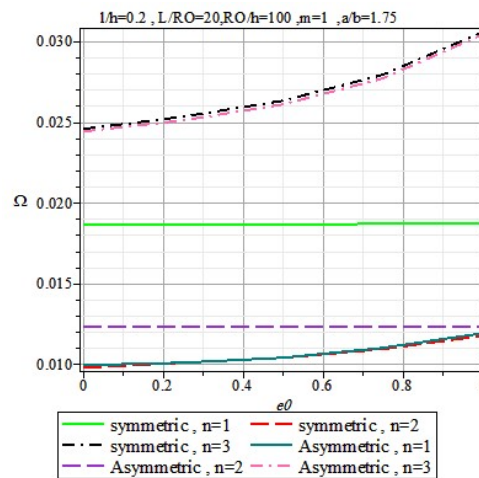


Figure 16: The dimensionless natural frequency of the porous elliptical microshell versus porosity parameters for different values of circumferential wave numbers in symmetric and asymmetric modes.

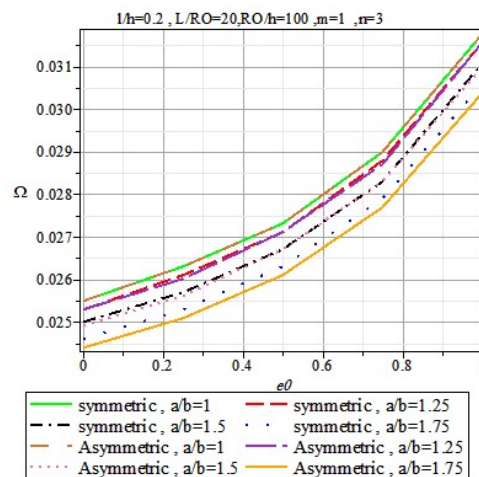


Figure 17: The dimensionless natural frequency of the elliptical microshell versus porosity parameters for diverse values of  $a/b$  in symmetrical and asymmetrical modes.

in the symmetrical mode are greater than those for the asymmetrical mode. Also, when the elliptical ratio ( $a/b$ ) is equal to one, the natural frequencies for both the symmetrical and asymmetrical modes are equal. To justify this phenomenon, it is assumed that  $a/b$  is equal to one; the cross-section of the microshell converts to a circle.

As shown in Fig. 18, the natural frequencies of elliptical microshells behave differently by increasing  $a/b$  at various circumferential wave numbers. For odd numbers, the values of the natural frequency of the microshell in the symmetrical mode are greater than in those in the asymmetrical mode. Also, for even circumferential wave numbers,

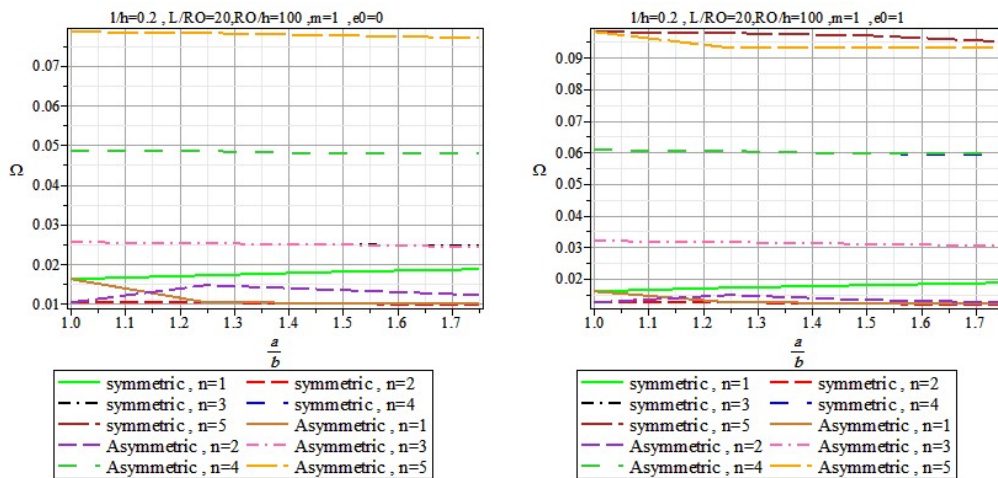


Figure 18: The dimensionless natural frequency of the elliptical microshell equal to  $a/b$  for different values of circumferential wave numbers in symmetrical and asymmetrical modes.

the natural frequencies of the elliptical microshell are lower in the symmetrical mode than that of the asymmetrical mode. This is more significant for the smaller circumferential wave numbers than for the larger numbers. In general, the natural frequency of the elliptical microshell decreases by increasing  $a/b$  because the elliptical parameters lower the shell's stiffness.

Table 9 shows the natural frequency of the elliptical microshell for various values of porosity and its distribution patterns in a symmetrical mode. The corresponding diagram is plotted in Fig. 19.

By growing the porosity values, for porosity distribution type 1 (symmetrical), the natural frequency of the elliptical microshell increases; however, it decreases for the distribution type 2 (asymmetrical). This phenomenon is due to variation in the material stiffness of the microshell. By increasing the porosity parameter for distribution type 1 (symmetrical), the material stiffness of the microshell rises, causing the natural frequency to rise. Although, for porosity distribution type 2 (asymmetrical), an increase in poros-

Table 9: The dimensionless natural frequency of the elliptical microshells for various values of porosity and its distribution in a symmetrical mode.

Symmetric		$\Omega = \omega R_0 \sqrt{\frac{\rho_0(1-\nu^2)}{E_0}}, n=1, \frac{a}{b}=1.4, \frac{L}{R_0}=20, \frac{R_0}{h_1}=100, \frac{l}{h}=0.5, h_2=0$								
		$e_0=0$	$e_0=0.1$	$e_0=0.2$	$e_0=0.3$	$e_0=0.4$	$e_0=0.5$	$e_0=0.6$	$e_0=0.7$	$e_0=0.8$
Dist type 1	$n=1$	0.0178	0.0178	0.0178	0.0178	0.0178	0.0178	0.0178	0.0178	0.0178
	$n=2$	0.0147	0.0148	0.0148	0.0149	0.0150	0.0151	0.0152	0.0154	0.0156
	$n=3$	0.0383	0.0385	0.0387	0.0390	0.0392	0.0395	0.0399	0.0404	0.0410
Dist type 2	$n=1$	0.0178	0.0178	0.0178	0.0178	0.0178	0.0178	0.0178	0.0178	0.0178
	$n=2$	0.0147	0.0147	0.0147	0.0147	0.0147	0.0147	0.0146	0.0146	0.0144
	$n=3$	0.0383	0.0384	0.0384	0.0384	0.0384	0.0383	0.0381	0.0379	0.0374

ity distribution lowers the structure’s stiffness. As a result, the natural frequency of the microshell drops.

### 3.5 The porous elliptical microshell with an MRF core

In this section, the effects of different parameters on natural frequency and loss factor of the elliptical microshell (MRF) core are presented and discussed. The parameters consist of material length scale, porosity, geometry of the microshell, longitudinal and circumferential wave numbers, and the magnetic field intensity. Table 10 presents the natural frequency and the loss factor of the elliptical microshell for various values of  $a/b$  and  $h_2/h_1$  in the symmetrical mode. The corresponding diagrams are presented in Figs. 20 and 21.

As shown in Fig. 20, by increasing the value of  $h_2/h_1$ , the natural frequency of the elliptical decreases for all values of the circumferential wave numbers. This occurs because as the core thickness increases, the stiffness of the shell declines.

As shown in Fig. 21, the minimum loss factor occurs at  $h_2/h_1 = 1$ . The loss factor increases by increasing or decreasing the  $h_2/h_1$  ratio compared to when the  $h_2/h_1$  is equal to one. Table 11 presents the values of the natural frequency and loss factor for

Table 10: The natural frequency and loss factor of the elliptical microshell for various values of  $a/b$  and  $h_2/h_1$  in a symmetrical mode.

Symmetrical Mode			$\omega = \sqrt{\text{Re}(\Omega^2)}, \eta = \frac{\text{Im}(\Omega^2)}{\text{Re}(\Omega^2)}$						
			$e_0 = 0.5, B = 100, \frac{l}{R_0} = 2, \frac{R_0}{h_1} = 50, \frac{l}{h_1} = 0.5, m = 1, \text{dist type} = 1$						
			$h_2/h_1 = 1/4$	$h_2/h_1 = 1/2$	$h_2/h_1 = 3/4$	$h_2/h_1 = 1$	$h_2/h_1 = 4/3$	$h_2/h_1 = 2$	$h_2/h_1 = 4$
$a/b = 1$	$n = 1$	$\omega \times 10^{-6}$	29.881	28.812	27.850	26.978	25.934	24.164	20.456
		$\eta \times 10^6$	29.432	21.297	19.053	18.326	18.514	19.993	27.008
	$n = 2$	$\omega \times 10^{-6}$	17.213	16.594	16.039	15.537	14.936	13.917	11.783
		$\eta \times 10^6$	219.33	155.95	138.81	133.71	134.06	144.04	192.73
	$n = 3$	$\omega \times 10^{-6}$	11.230	10.819	10.456	10.128	9.736	9.073	7.686
		$\eta \times 10^6$	1064.50	760.99	682.56	661.82	668.18	724.87	982.94
$a/b = 1.2$	$n = 1$	$\omega \times 10^{-6}$	32.445	31.283	30.239	29.293	28.159	26.238	22.211
		$\eta \times 10^6$	21.988	15.787	14.058	13.539	13.577	14.611	19.656
	$n = 2$	$\omega \times 10^{-6}$	16.827	16.222	15.68	15.189	14.60	13.605	11.519
		$\eta \times 10^6$	244.28	173.64	154.60	148.97	149.42	160.65	215.15
	$n = 3$	$\omega \times 10^{-6}$	10.924	10.524	10.170	9.85	9.470	8.825	7.477
		$\eta \times 10^6$	1140.36	817.79	735.07	713.87	721.86	784.72	1066.94
$a/b = 1.4$	$n = 1$	$\omega \times 10^{-6}$	34.376	33.145	32.035	31.037	29.835	27.800	23.534
		$\eta \times 10^6$	17.097	12.277	11.068	10.892	10.834	11.567	15.428
	$n = 2$	$\omega \times 10^{-6}$	15.950	15.375	14.862	14.396	13.839	12.895	10.918
		$\eta \times 10^6$	311.83	226.80	196.71	191.17	192.18	207.24	278.76
	$n = 3$	$\omega \times 10^{-6}$	10.337	9.957	9.622	9.321	8.960	8.350	7.075
		$\eta \times 10^6$	1283.54	930.32	831.07	810.76	821.61	895.72	1222.50
$a/b = 1.6$	$n = 1$	$\omega \times 10^{-6}$	35.665	34.389	33.241	32.200	30.954	28.842	24.416
		$\eta \times 10^6$	8.990	6.417	5.666	5.428	5.424	5.829	7.880
	$n = 2$	$\omega \times 10^{-6}$	14.523	13.999	13.531	13.107	12.600	11.741	9.942
		$\eta \times 10^6$	401.60	288.84	259.82	252.42	255.35	277.81	378.63
	$n = 3$	$\omega \times 10^{-6}$	9.851	9.483	9.162	8.875	8.532	7.953	6.743
		$\eta \times 10^6$	323725	324010	324073	324080	324057	323972	323629

Table 11: The natural frequency and loss factor of the elliptical microshell for different values of porosity and  $l/h$  in a symmetrical mode.

Symmetrical Mode			$\omega = \sqrt{\text{Re}(\Omega^2)}, \eta = \frac{\text{Im}(\Omega^2)}{\text{Re}(\Omega^2)}$									
			$a/b = 1.4, B = 300, \frac{L}{R_0} = 5, \frac{R_0}{h_1} = 100, \frac{h_2}{h_1} = 1, m = 1$									
			$e_0 = 0$		$e_0 = 0.2$		$e_0 = 0.4$		$e_0 = 0.6$		$e_0 = 0.8$	
			Type1	Type2	Type1	Type2	Type1	Type2	Type1	Type2	Type1	Type2
$l/h = 0$	$n = 1$	$\omega$	5.03	5.03	4.97	4.97	4.88	4.88	4.77	4.77	4.62	4.61
		$\eta$	19.12	19.12	20.29	20.73	22.19	22.95	25.03	26.78	29.36	43.72
	$n = 2$	$\omega$	1.78	1.78	1.76	1.76	1.73	1.73	1.70	1.69	1.66	1.63
		$\eta$	1906.8	1906.8	2208.4	2100.0	2639.3	2320.9	3317.0	2556.3	4578.5	2759.4
	$n = 3$	$\omega$	1.06	1.06	1.06	1.05	1.06	1.03	1.06	1.01	1.06	0.96
		$\eta$	11543	11543	12767	12535.4	14283.8	13722.1	16210.8	15185.5	18730.3	17133.6
$l/h = 1/4$	$n = 1$	$\omega$	5.03	5.03	4.97	4.97	4.88	4.88	4.77	4.77	4.62	4.62
		$\eta$	17.10	17.10	19.15	18.74	21.85	20.69	25.72	23.02	27.65	25.97
	$n = 2$	$\omega$	1.81	1.81	1.79	1.78	1.77	1.75	1.74	1.71	1.70	1.65
		$\eta$	2341.70	2341.70	2781	2596	3441	2882	4541	3161	5472	3311
	$n = 3$	$\omega$	1.13	1.13	1.13	1.12	1.13	1.11	1.13	1.08	1.13	1.04
		$\eta$	9933.0	9933.0	11046	10805	12438	11841	14225	13095	16789	14671
$l/h = 1/2$	$n = 1$	$\omega$	5.03	5.03	4.97	4.97	4.88	4.88	4.77	4.77	4.62	4.62
		$\eta$	16.95	16.95	19.00	18.58	21.64	20.51	25.18	22.79	30.23	25.35
	$n = 2$	$\omega$	1.70	1.70	1.68	1.68	1.66	1.65	1.63	1.61	1.59	1.55
		$\eta$	2866.88	2866.88	3079.9	3090.3	3326.5	3370.7	3619.4	3757.2	3984.5	4420.7
	$n = 3$	$\omega$	1.34	1.34	1.33	1.32	1.32	1.30	1.31	1.27	1.30	1.22
		$\eta$	7106.25	7106.25	7960.2	7749.4	9045.3	8508.3	10468	9408.5	12410	10474.7

the elliptical microshell at different porosity values and  $l/h$  in a symmetrical mode. The corresponding diagrams are illustrated in Figs. 22 and 23.

Fig. 22 indicates that the natural frequency of the elliptical microshell decreases by increasing the porosity values. The reduction is higher for the distribution type 2 than for the type 1. Also, as seen in Fig. 23, by increasing the porosity, the values of the loss

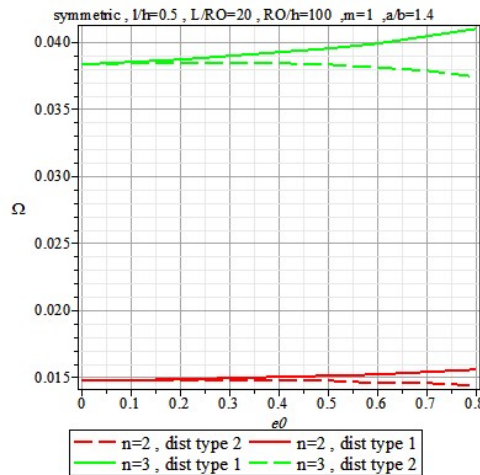


Figure 19: The dimensionless natural frequency of the elliptical microshells for different values of porosity parameters and its distribution in a symmetrical mode.

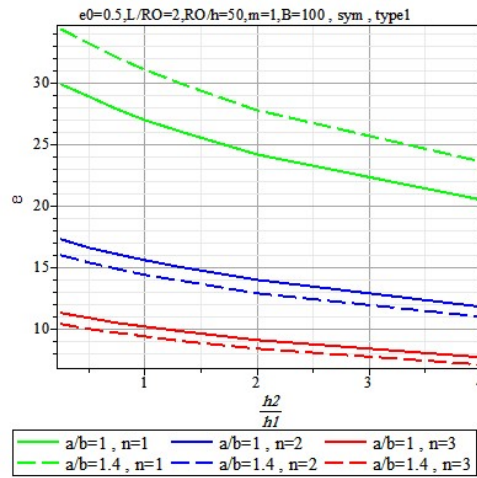


Figure 20: The natural frequency of the elliptical microshells for different values of  $a/b$  and  $h_2/h_1$  in a symmetrical mode.

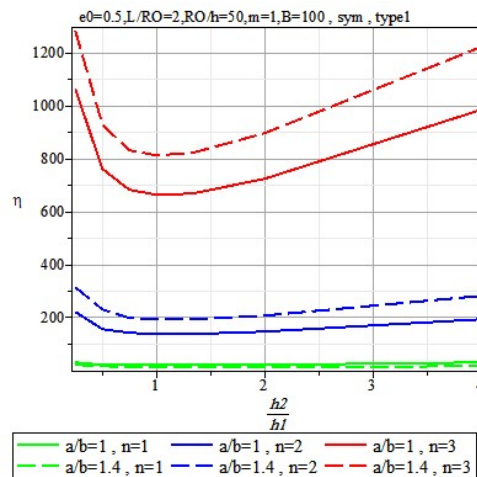


Figure 21: The loss factor values of the elliptical microshell for various values of  $a/b$  and  $h_2/h_1$  in a symmetrical mode.

factor for the elliptical microshell increase. The growth in the porosity distribution type 1 is higher than that for the type 2. Table 12 presents the natural frequency and the loss factor of the elliptical microshell for different values of the magnetic field intensity and  $a/b$  ratio in symmetrical and asymmetrical modes. The corresponding diagram is presented in Fig. 24. As shown in Fig. 24, by raising the magnetic field intensity from 0 to 400G, the loss factor of the microshell increases. However, increasing the magnetic intensity beyond 400G, the loss factor begins to decline.

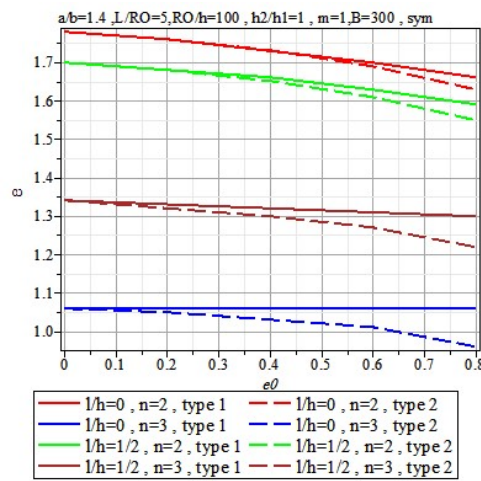


Figure 22: The natural frequency of the elliptical microshells for various values of porosity and  $l/h$  ratios in a symmetrical mode.

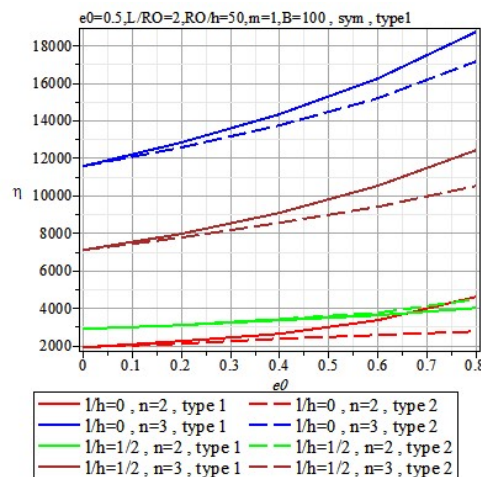


Figure 23: The loss factor values of the elliptical microshells for different values of porosity and  $l/h$  in a symmetrical mode.

## 4 Conclusions

Based on the study's data, the following conclusions may be drawn:

1. As the length scale increases, the natural frequencies of the microshells remains constant for  $n = 1$  and increases for  $n > 1$ .
2. The effect of length scale on the natural frequency is greater at higher values of the circumferential wave numbers.

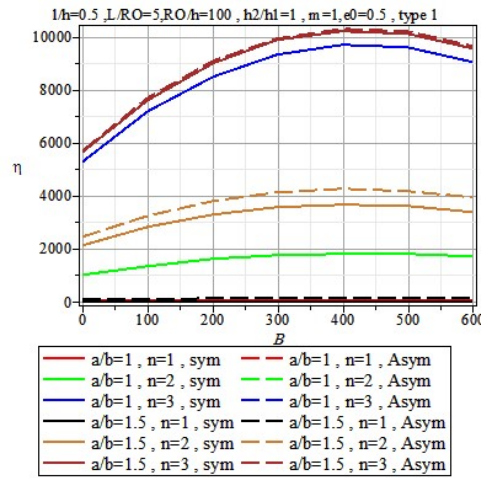


Figure 24: The loss factor values of the elliptical microshells for various values of the magnetic field intensity and  $a/b$  in symmetrical and asymmetrical modes.

Table 12: The natural frequency and loss factor of the elliptical microshell for different values of the magnetic field intensity and  $a/b$  in symmetrical and asymmetrical modes.

Magnetic Intensity?	$\omega = \sqrt{\text{Re}(\Omega^2)}, \eta = \frac{\text{Im}(\Omega^2)}{\text{Re}(\Omega^2)}$															
	$l/h = 0.5, \epsilon_0 = 0.5, \frac{l}{R_0} = 5, \frac{R_0}{h_1} = 100, \frac{h_2}{h_1} = 1, m = 1, \text{dist type} = 1$															
	B=0		B=100		B=200		B=300		B=400		B=500		B=600			
	sym	asym	sym	asym	sym	asym	sym	asym	sym	asym	sym	asym	sym	Asym		
$a/b=1$	$n=1$	$\omega$	4.39	4.39	4.39	4.39	4.39	4.39	4.39	4.39	4.39	4.39	4.39	4.39	4.39	
		$\eta$	16.57	16.57	21.07	21.07	23.74	23.74	25.03	25.03	25.21	25.21	24.44	24.44	22.78	22.78
	$n=2$	$\omega$	1.83	1.83	1.83	1.83	1.83	1.83	1.83	1.84	1.84	1.84	1.84	1.84	1.84	1.84
		$\eta$	1004.17	1004.17	1355.83	1355.83	1601.95	1601.95	1752.88	1752.88	1816.01	1816.01	1796.27	1796.27	1696.40	1696.40
	$n=3$	$\omega$	1.35	1.35	1.36	1.36	1.36	1.36	1.37	1.37	1.37	1.37	1.38	1.38	1.38	1.38
		$\eta$	5301.20	5301.20	7179.77	7179.77	8505.49	8505.49	9327.11	9327.11	9679.76	9679.76	9586.85	9586.85	9061.39	9061.39
$a/b=1.25$	$n=1$	$\omega$	4.70	4.02	4.70	4.02	4.70	4.02	4.70	4.02	4.70	4.02	4.70	4.02	4.70	4.02
		$\eta$	13.89	28.51	17.93	36.93	20.47	42.26	21.82	45.14	22.17	45.94	21.63	44.88	20.25	42.06
	$n=2$	$\omega$	1.73	1.74	1.73	1.75	1.73	1.75	1.74	1.75	1.74	1.76	1.74	1.76	1.74	1.76
		$\eta$	1905.11	2059.61	2516.39	2716.49	2920.30	3148.19	3149.94	3391.64	3227.55	3471.74	3167.02	3404.06	2975.59	3196.70
	$n=3$	$\omega$	1.32	1.32	1.33	1.33	1.34	1.34	1.35	1.34	1.35	1.35	1.35	1.35	1.36	1.35
		$\eta$	5408.02	5409.57	7319.85	7321.59	8667.09	8668.81	9500.61	9502.19	9856.89	9858.28	9760.21	9761.39	9223.99	9225.00
$a/b=1.5$	$n=1$	$\omega$	4.91	3.71	4.91	3.71	4.91	3.71	4.91	3.71	4.91	3.71	4.91	3.71	4.91	3.71
		$\eta$	0.46	73.28	0.55	99.34	0.56	118.14	0.62	130.24	0.67	135.88	0.71	135.20	0.70	128.21
	$n=2$	$\omega$	1.58	1.63	1.58	1.63	1.59	1.64	1.59	1.64	1.59	1.64	1.59	1.64	1.59	1.64
		$\eta$	2117.56	2448.29	2819.00	3259.90	3292.29	3806.84	3568.96	4125.79	3670.77	4242.36	3611.71	4173.09	3399.25	3926.91
	$n=3$	$\omega$	1.27	1.27	1.28	1.28	1.29	1.29	1.30	1.29	1.30	1.30	1.31	1.30	1.31	1.30
		$\eta$	5635.38	5683.85	7618.14	7681.52	9010.48	9084.33	9869.01	9948.51	10232.91	10314.13	10128.14	10207.65	9569.02	9643.64

- The effect of length scale ( $l/h$ ) on the natural frequency rises by increasing the elliptical ratio ( $a/b$ ). At higher values of  $a/b$ , the effect of  $l/h$  on the natural frequency is more pronounced.
- The natural frequency varies for various circumferential wave numbers. For  $n = 1$ , by increasing  $a/b$ , the natural frequency grows, and for  $n > 1$ , it follows an opposite trend.
- The value of the structure's length scale influences the variation of the natural frequency versus that of the  $a/b$ .

6. At low values of  $l/h$  and increases in  $a/b$ , the trend in the natural frequency variation is downward. At higher values of  $l/h$ , the variations in the natural frequency increases when the  $a/b$  values rise.
7. In the classical theory ( $l/h=0$ ), when the circumferential wave number increases from  $n=1$  to  $n=2$ , the natural frequency declines. For  $n>1$ , the natural frequency rises; however, at large values of the length scale, the natural frequency increases consistent with increases in the circumferential wave numbers.
8. As the porosity increases, the natural frequency remains fairly constant for  $n=1$  but it increases for  $n>1$ . Also, the effect of the porosity on the rise in the natural frequency is greater at the higher values of the circumferential wave numbers.
9. For  $n=1$ , an increase in  $a/b$  raises the natural frequency of the microshell. For  $n>1$ , the natural frequency declines by increases in the  $a/b$  ratio.
10. As  $R_o/h$  increases, the natural frequency remains fairly constant for  $n=1$  but declines for  $n>1$ .
11. For circumferential wave numbers, at  $n=1$  and 3, the natural frequency values are higher in symmetrical mode than in the asymmetrical one. However, at  $n=2$ , the trend is opposite.
12. The differences between the symmetrical and asymmetrical modes decline by increases in the circumferential wave numbers.
13. As the ellipse ratio  $a/b$  approaches one, the natural frequency value of the microshell in the symmetrical mode is similar to that of the asymmetrical mode. This occurs because at  $a/b=1$  turns the cross-section of the microshell close to a circle.
14. For odd values of the circumferential wave numbers, the natural frequency in symmetrical mode is greater than that of the asymmetrical mode. For even circumferential wave numbers, the natural frequency in symmetrical mode is lower than that for the asymmetrical mode. The difference is more pronounced for smaller values of the circumferential wave numbers than for the larger values.
15. The natural frequency decreases by increasing the elliptical radii ( $a/b$  ratio).
16. By raising the porosity values, the natural frequency increases in distribution type 1 (symmetrical) but decreases in distribution type 2 (asymmetrical).
17. For all values of the circumferential wave numbers, increasing the  $h_2/h_1$  ratio, the natural frequency declines.
18. For  $h_1/h_2=1$ , the value of loss factor is at a minimum. But for other values of  $h_2/h_1$  ratio, the loss factor tends to rise.

19. By increasing the porosity values, the loss factor grows. This increase is higher for the distribution type 1 than for that of type 2.
20. The loss factor increases by raising the magnetic field intensity from 0 to 400G while it declines at the intensities higher than 400G.

## References

- [1] A. LEISSA, *Vibration of Shells: Scientific and Technical Information Office, National Aeronautics and Space Administration: United States Government Printing Office, Washington, D.C., 1973.*
- [2] M. QUATO, *Recent research advances in the dynamic behavior of shells: 1989-2000, Part 1: Laminated composite shells*, Appl. Mech. Rev., 55 (2002), pp. 325–350.
- [3] K. SHIRAKAWA AND M. MORITA, *Vibration and buckling of cylinders with elliptical cross section*, J. Sound Vib., 84 (1982), pp. 121–131.
- [4] J. KLOSNER, *Frequencies of an Infinitely Long Noncircular Cylindrical Shell: Part 2., Plane Strain, Torsional and Flexural Modes: Polytechnic Institute of Brooklyn, Department of Aeronautical Engineering, 1959.*
- [5] J. KLOSNER AND F. POHLE, *Natural Frequencies of an Infinitely Long Noncircular Cylindrical Shell: Polytechnic Institute of Brooklyn, Department of Aeronautical Engineering, 1958.*
- [6] G. YAMADA, T. IRIE AND S. NOTOYA, *Natural frequencies of elliptical cylindrical shells*, J. Sound Vib., 101 (1985), pp. 133–139.
- [7] K. SUZUKI, G. SHIKANAI AND A. LEISSA, *Free vibrations of laminated composite non-circular thick cylindrical shells*, Int. J. Solids Struct., 33 (1996), pp. 4079–4100.
- [8] M. GANAPATHI, B. PATEL AND H. PATEL, *Free flexural vibration behavior of laminated angle-ply elliptical cylindrical shells*, Comput. Struct., 82 (2004), pp. 509–518.
- [9] A. GRIGORENKO, S. PUZYREV AND E. VOLCHEK, *Investigation of free vibrations of noncircular cylindrical shells by the spline-collocation method*, J. Math. Sci., 185 (2012), pp. 824–836.
- [10] A. KHALIFA, *Solving the vibration problem of inhomogeneous orthotropic cylindrical shells with hoop-corrugated oval cross section*, Comptes Rendus Mécanique, 343 (2015), pp. 482–494.
- [11] M. KHALIFA, *Effects of non-uniform Winkler foundation and non-homogeneity on the free vibration of an orthotropic elliptical cylindrical shell*, Euro. J. Mech. A/Solids, 49 (2015), pp. 570–581.
- [12] F. TORNABENE, N. FANTUZZI, M. BACCIOCCHI AND R. DIMITRI, *Dynamic analysis of thick and thin elliptic shell structures made of laminated composite materials*, Compos. Struct., 133 (2015), pp. 278–299.
- [13] F. TORNABENE, N. FANTUZZI, M. BACCIOCCHI AND R. DIMITRI, *Free vibrations of composite oval and elliptic cylinders by the generalized differential quadrature method*, Thin-Walled Struct., 97 (2015), pp. 114–129.
- [14] J. REDDY AND C. CHIN, *Thermomechanical analysis of functionally graded cylinders and plates*, J. Therm. Stresses, 21 (1998), pp. 593–626.
- [15] C. LOY, K. LAM AND J. REDDY, *Vibration of functionally graded cylindrical shells*, Int. J. Mech. Sci., 41 (1999), pp. 309–324.
- [16] S. PRADHAN, C. LOY, K. LAM AND J. REDDY, *Vibration characteristics of functionally graded cylindrical shells under various boundary conditions*, Appl. Acoust., 61 (2000), pp. 111–129.

- [17] B. PATEL, S. GUPTA, M. LOKNATH AND C. KADU, *Free vibration analysis of functionally graded elliptical cylindrical shells using higher-order theory*, Compos. Struct., 69 (2005), pp. 259–270.
- [18] F. EBRAHIMI AND M. MOKHTARI, *Transverse vibration analysis of rotating porous beam with functionally graded microstructure using the differential transform method*, Journal of the Brazilian Society of Mechanical Sciences and Engineering, 37 (2015), pp. 1435–1444.
- [19] F. EBRAHIMI AND M. ZIA, *Large amplitude nonlinear vibration analysis of functionally graded Timoshenko beams with porosities*, Acta Astronautica, 116 (2015), pp. 117–125.
- [20] A. ERINGEN, *Theory of micropolar plates*, Zeitschrift für Angewandte Mathematik und Physik ZAMP, 18 (1967), pp. 12–30.
- [21] A. ERINGEN, *Nonlocal polar elastic continua*, Int. J. Eng. Sci., 10 (1972), pp. 1–16.
- [22] M. GURTIN, J. WEISSMÜLLER AND F. LARCHE, *A general theory of curved deformable interfaces in solids at equilibrium*, Philosophical Magazine A, 78 (1998), pp. 1093–1109.
- [23] E. AIFANTIS, *Strain Gradient Interpretation of Size Effects*, Fracture Scaling: Springer, (1999), pp. 299–314.
- [24] F. YANG, A. CHONG, D. LAM, AND P. TONG, *Couple stress based strain gradient theory for elasticity*, Int. J. Solids Struct., 39 (2002), pp. 2731–2743.
- [25] S. COSKUN, J. KIM, AND H. TOUTANJI, *Bending, free vibration, and buckling analysis of functionally graded porous micro-plates using a general third-order plate theory*, J. Compos. Sci., 3(1) (2019), p. 15.
- [26] J. KIM, K. ŽUR AND J. REDDY, *Bending, free vibration, and buckling of modified couples stress-based functionally graded porous micro-plates*, Compos. Struct., 209 (2019), pp. 879–888.
- [27] M. GHADIRI AND H. SAFARPOUR, *Free vibration analysis of size-dependent functionally graded porous cylindrical microshells in thermal environment*, J. Therm. Stresses, 40 (2017), pp. 55–71.
- [28] H. AFSHARI AND N. ADAB, *Size-dependent buckling and vibration analyses of GNP reinforced microplates based on the quasi-3D sinusoidal shear deformation theory*, Mechanics Based Design of Structures and Machines, (2020), pp. 1–22.
- [29] N. ADAB, M. AREFI AND M. AMABILI, *A comprehensive vibration analysis of rotating truncated sandwich conical microshells including porous core and GPL-reinforced face-sheets*, Compos. Struct., 279 (2021), p. 114761.
- [30] H. ZEIGHAMPOUR AND Y. BENI, *Cylindrical thin-shell model based on modified strain gradient theory*, Int. J. Eng. Sci., 78 (2014), pp. 27–47.
- [31] G. ZHANG, T. LI, X. ZHU, J. YANG AND Y. MIAO, *Free and forced vibration characteristics of submerged finite elliptic cylindrical shell*, Ocean Eng., 129 (2017), pp. 92–106.
- [32] Y. XIANG, Y. HUANG, J. LU, L. YUAN AND S. ZOU, *New matrix method for analyzing vibration and damping effect of sandwich circular cylindrical shell with viscoelastic core*, Appl. Math. Mech., 29 (2008), pp. 1587–1600.
- [33] K. SOLDATOS, *On thickness shear deformation theories for the dynamic analysis of non-circular cylindrical shells*, Int. J. Solids Struct., 22 (1986), pp. 625–641.
- [34] M. AHMED, *Simplified equations and solutions for the free vibration of an orthotropic oval cylindrical shell with variable thickness*, Math. Methods Appl. Sci., 34 (2011), pp. 1789–1800.
- [35] M. GANAPATHI, B. PATEL, H. PATEL AND D. PAWARGI, *Vibration analysis of laminated cross-ply oval cylindrical shells*, J. Sound Vib., 262 (2003), pp. 65–86.
- [36] R. TOUPIN, *Elastic materials with couple-stresses*, Arch. Ration. Mech. Anal., 11 (1962), pp. 385–414.
- [37] R. MINDLIN, *Micro-structure in linear elasticity*, Arch. Ration. Mech. Anal., 16 (1964), pp. 51–78.

- [38] R. MINDLIN AND H. TIERSTEN, *Effects of couple-stresses in linear elasticity*, Arch. Ration. Mech. Anal., 11 (1962), pp. 415–448.
- [39] W. KOITER, *Couple stresses in the theory of elasticity: I and II*, Philosophical Transactions of the Royal Society of London B, 67 (1964), pp. 17–44.
- [40] R. MINDLIN, *Second gradient of strain and surface-tension in linear elasticity*, Int. J. Solids Struct., 1 (1965), pp. 417–438.
- [41] N. FLECK AND J. HUTCHINSON, *Strain gradient plasticity*, Adv. Appl. Mech., 33 (1997), pp. 295–361.
- [42] F. YANG, A. CHONG AND D. LAM ET AL., *Couple stress based strain gradient theory for elasticity*, Int. J. Solids Struct., 39 (2002), pp. 2731–2743.
- [43] R. GHOLAMI AND R. ANSARI, *Size-dependent geometrically nonlinear free vibration of first-order shear deformable piezoelectric-piezomagnetic nanobeams using the nonlocal theory*, Adv. Appl. Math. Mech., 10 (2018), pp. 184–208.
- [44] M. JALAEI AND O. CIVALEK, *On viscoelastic transient response of magnetically imperfect functionally graded nanobeams*, Int. J. Eng. Sci., 172 (2022), p. 103629.
- [45] O. CIVALEK AND S. AKBAS ET AL., *Forced vibration analysis of composite beams reinforced by carbon nanotubes*, Nanomaterials, 11(3) (2021), p. 571.
- [46] K. LIEW AND C. LIM, *Vibratory characteristics of cantilevered rectangular shallow shells of variable thickness*, AIAA J., 32(2) (1994), pp. 387–396.
- [47] I. SOLEIMANI, Y. TADI AND F. MEHRALIAN, *A new size-dependent cylindrical shell element based on modified couple stress theory*, Adv. Appl. Math. Mech., 10 (2018), pp. 819–844.